

Method to deterministically generate large-amplitude optical cat states

Zheng-Hong Li,^{1,2,*} Fei Yu,¹ Zhen-Ya Li,¹ M. Al-Amri,^{3,4,5,*} and M. Suhail Zubairy^{3,*}

1 Department of Physics, Shanghai University, Shanghai 200444, China

2 Shanghai Key Laboratory of High Temperature Superconductors, Shanghai University, Shanghai 200444, China

3 Institute for Quantum Science and Engineering (IQSE) and Department of Physics and Astronomy, Texas A&M University, College Station, Texas 77843-4242, USA

4 NCQQQI, KACST, P.O.Box 6086, Riyadh 11442, Saudi Arabia

5 Institute of Quantum Technologies and Advanced Computing, KACST, Riyadh 11442, Saudi Arabia

A deterministic preparation method for large-amplitude optical cat state is proposed. The key ingredient is to generate entanglement between macro and micro systems by utilizing interaction-free measurement and quantum Zeno effect. Our method enables the quantum microsystem to gently manipulate strong light field without directly interacting with it. The direct interaction is bypassed by multiple interactions, each of which has only a small fraction of photons interacting with the quantum microsystem. Therefore, our method allows the quantum microsystem to function entirely within a weak field environment, which is a distinct advantage of our method. Moreover, we also show that the cat state preparation can be achieved even if the quantum microsystem suffers from large photon loss, as long as optical losses from classical devices remain low. We use a cavity-atom coupling system to illustrate the quantum microsystem. We demonstrate that as the number of interactions increases, our scheme becomes less and less sensitive to both atomic spontaneous emission and detuning between the atom and the cavity. Therefore, the fidelity of the cat state can be increased by improving and perfecting the classical optical system.

I. Introduction

Schrödinger's gedanken experiment involving a cat in a superposition of dead and alive states vividly demonstrates the magical picture of quantum superposition on a macro scale [1]. In modern physics, this cat state (CS) is usually represented by the superposition of two distinct coherent states $|\pm\alpha\rangle$. With the increase of amplitude $|\alpha|$, CS gets closer to the macroscopic superposition. It is not only attractive from a fundamental point of view [2,3], but also valuable for applications including quantum teleportation [4-7], quantum computing [8-13], quantum error correction [14-17] and quantum metrology [18-24]. After decades of efforts, now CS has been generated on various platforms [3,25-28]. However, in the optical domain, in the best experimental results so far, $|\alpha|$ remains less than 2 [29-37]. Moreover, it is still challenging to further increase the value of $|\alpha|$ based on existing methods. For example, the widely studied photon subtraction method [29-33,38,39], which is a probabilistic method based on post-selection, has low probability of success for generating large-amplitude CS. Another approach that has attracted a lot of attention is the synthesis method [36,40,41], which uses a pre-prepared CS as a seed to grow large-amplitude CS. Therefore, this method is still limited by the amplitude of the pre-prepared CS. Furthermore, there was an old deterministic method that based on light-matter interaction [42], which has recently been done experimentally [37]. In this method, CS is generated by direct interaction between an incident coherent light pulse and a single-side cavity containing a three-level atom [37,42-45]. Its basic idea is to use normal-mode splitting [43] to

control the phase of the reflected coherent light field. In the experiment, the amplitude of the output CS is $|\alpha| \approx 1.4$ [37]. Unfortunately, this method is limited from preparing arbitrarily large $|\alpha|$ CS for a given optical pulse length since such atom-cavity coupling system is fragile when it interacts with strong light field. This is because single atom cannot handle the strong field, which leads strong field to get into the cavity and be reflected just like the case of the empty cavity. Needless to say, optical field is an excellent medium for information transmission. Considering the practical application requirements that involve integrating diverse quantum systems, as well as for advanced sensing and imaging techniques, the generation of optical CS with large amplitudes and customizable propagation properties becomes not only necessary but also of significant value. This endeavor represents a pioneering frontier in the realm of quantum optics, bearing profound implications for both the theoretical understanding and the advancement of practical quantum technology [46].

In this article, we propose a deterministic method to generate flying optical CS whose amplitude can be arbitrarily large, provided that optical losses from classical optical devices remain low. The key step of our scheme is to entangle a strong coherent light field with a microscopic quantum system prepared in a superposition state initially. After the entanglement, the optical CS is obtained by performing projection measurement on the quantum microsystem. However, in response to the situation that a quantum microsystem is typically very fragile when it interacts with strong light fields, our solution can ensure that such fragile microsystem can resist and control strong field without directly interacting with it. The basic idea comes from interaction-free measurement based on quantum Zeno effect [47-49], which is considered a powerful non-invasive measurement method that can protect vulnerable samples. In this work, we further apply it to protect the quantum properties of a fragile microscopic system from being destroyed by strong fields. We replace direct interaction between strong light field and the microsystem by a sequence of interactions, each with only a small fraction of photons actually interacting with the microsystem. This leads to the fact that the quantum microsystem always works in a weak field environment, which is one of the main advantages of this work. Eliminating the negative influence of strong fields gives liberty of applying this method in a wide variety of systems and provides the potential for future applications. More importantly, this indicates that our scheme allows quantum microscopic systems to manipulate macroscopic counterparts that are challenging to control directly. In addition, our method has another important advantage—it can reduce the requirements of quantum microscopic systems. For illustration, we employ the single-side cavity-atom coupling model used in Ref. [37] as our specific quantum microscopic subsystem. Our simulation shows that our scheme becomes less and less sensitive to both atomic spontaneous emission and detuning between the atom and the cavity as the number of interactions increases, when other classical optical devices are ideal. We observe that spontaneous emission decay induces optical losses. Utilizing quantum Zeno effect, our approach provides a unique solution to mitigate the impact of such optical losses originating from quantum device (referred to as Type I light loss), without the need for improving the quantum microscopic system. In other words, our scheme is only sensitive to optical losses introduced by classical optical devices (referred to as Type II light loss). Finally, it is also worth mentioning that here we mainly focus on the optical platform, but our approach can also be extended to other platforms such as superconducting microwave resonator [50,51].

II. Results

A. General multiple reflection scheme

First, we focus on explaining the principle of our method. More detailed experimental protocols will be discussed later. We start with the chain Mach-Zehnder interferometer shown in Fig. 1a, which is a commonly used optical structure for interaction-free measurement [52-57]. Compared to conventional interaction-free measurement studies, our scheme has two distinct features, although these are commonly used and even necessary for CS preparation. Firstly, we use the coherent light source (S) instead of single photon light source. Secondly, conventional interaction-free measurement only assume that an object has two functions: absorbing and transmitting any photons passing through the object. However, our method includes another function for the object, which is applying a π phase to the light field passing through it. In details, as shown in Fig.1a, MR stands for normal mirror, and BS stands for beam-splitter. The interference occurs between the light fields in Zones 0 and 1, which are located on the lower and upper sides of BS , respectively, separated by a dotted line. Assuming that a_z^\dagger ($z = 0,1$) represents the creation operator of the light field in Zone z , the function of BS can be described by $a_0^\dagger \rightarrow a_0^\dagger \cos \theta + a_1^\dagger \sin \theta$ and $a_1^\dagger \rightarrow a_1^\dagger \cos \theta - a_0^\dagger \sin \theta$ [49], where $\cos^2 \theta$ represents the reflectivity of BS . As for the object, it has three states, $|pass\rangle$, $|block\rangle$, and $|phase\rangle$. Firstly, we discuss the state $|pass\rangle$, where the object is transparent, thus the optical interference occurs continuously in Zones 0 and 1. Assuming the initial state of the light field is such that the field in Zone 0 is in coherent state $|\alpha\rangle$, while the field in Zone 1 is in the vacuum state $|0\rangle$, that is, $|\alpha, 0\rangle = \exp(\alpha a_0^\dagger - \alpha^* a_0)|0,0\rangle$. After passing through N number of BS s, it becomes $|\alpha \cos N\theta, \alpha \sin N\theta\rangle$ [58]. Apparently, when $\theta = \pi/2N$, we have $|0, \alpha\rangle$. While when $\theta = \pi/N$, we have $|-\alpha, 0\rangle$. The second state of the object is $|block\rangle$. In this case, any photon passing through the object is absorbed. Notice that the object and the light field interact many times. To take into account all absorbed photons, we write the state of the light field as $|C_0, C_1\rangle|l_1, l_2, \dots, l_{N-1}\rangle$, where $|C_{z=0,1}\rangle$ represents photon state in Zone z and $|l_1, l_2, \dots, l_{N-1}\rangle$ represents the photon absorbed each time. After the light pulse passing through the first BS , the initial state $|\alpha, 0\rangle|0,0, \dots, 0\rangle$ evolves to $|\alpha \cos \theta, \alpha \sin \theta\rangle|0,0, \dots, 0\rangle$, and it further becomes $|\alpha \cos \theta, 0\rangle|\alpha \sin \theta, 0, \dots, 0\rangle$ due to the absorption of the object. Subsequently, the photons remaining inside the interferometers pass through the next BS and interact with the object again. Such process repeats N times. After N numbers of BS s, the photon state is $|\alpha \cos^N \theta, \alpha \cos^{N-1} \theta \sin \theta\rangle \prod_{n=1}^{N-1} |\alpha \cos^{n-1} \theta \sin \theta\rangle$. Note that when $\theta = \pi/N$, we have $\cos^N \theta \rightarrow 1$ and $\sin \theta \rightarrow 0$ as $N \rightarrow \infty$. Therefore, as long as $|\alpha|^2$ is finite, the light field can be frozen in its initial state $|\alpha, 0\rangle|0,0, \dots, 0\rangle$. This also means that the actual number of photons absorbed by the object during the whole process is close to zero. Therefore, the object is protected from the strong light field due to the interruption of interference process in Zones 0 and 1. This is the quantum Zeno effect caused by photon loss. In addition to the state $|block\rangle$, there is another state of the object that also possesses the ability to sustain the light field in its initial state. This state is $|phase\rangle$, in which the object applies a π phase to the photons passing through it, i.e., $a_1^\dagger \rightarrow -a_1^\dagger$. When the photon passes through an odd number of BS , it becomes $|\alpha \cos \theta, \alpha \sin \theta\rangle$, while after passing through an even number of BS , it becomes $|\alpha, 0\rangle$. We note that the maximum intensity of the photons actually passing through the object in each interaction is $|\alpha \sin \theta|^2$. When $\theta = \pi/N$, its value tends to zero as N increases. This implies that under the condition of a large N , state $|phase\rangle$ can also result in the freezing of the light field. Consequently, for both states $|block\rangle$ and $|phase\rangle$, the object always works in a weak field environment.

Above, we have introduced the three states of the object and the corresponding dynamic evolution behavior of the light field. It is easy to see that if an object is initially in a superposition state of $(|pass\rangle + |block\rangle)/\sqrt{2}$ or $(|pass\rangle + |phase\rangle)/\sqrt{2}$, the object can be entangled with the coherent light field when $\theta = \pi/N$, i.e., $(|-\alpha, 0\rangle|pass\rangle + |\alpha, 0\rangle|block/phase\rangle)/\sqrt{2}$. After measuring the object with $(|pass\rangle \pm |block/phase\rangle)/\sqrt{2}$, CS can be deterministically created. However, whether it turns out to be an odd or even CS is random, each with a 50% probability of occurrence, depending on the measurement results. We have the even CS when the measurement result is $(|pass\rangle + |block/phase\rangle)/\sqrt{2}$. As for the other measurement result, the odd CS is obtained. We refer to the above method as the multiple reflection scheme since the optical field is reflected and interacts with the quantum object many times. In addition, it is worth mentioning that our method can also be used to realize the entangled coherent state $(|\alpha, 0\rangle + |0, \alpha\rangle)/\sqrt{2}$ required in Ref. [20,21]. To do so, we just need to set $\theta = \pi/2N$.

B. Multiple reflection scheme using single-side cavity-atom coupling system

The above is the basic idea of our method. The next important issue is to discuss what kind of a real quantum microscopic system that can be used as an object. We have shown that it is optional whether the object absorbs photons or provides a π phase. The difference is that the latter way does not introduce any photon loss. In theory, it has better fidelity. Therefore, in the rest of this paper, we will focus on a quantum microsystem which manipulates the photon phase. Nevertheless, given that photon loss due to device imperfection is inevitable in real systems, the former mechanism is also critical. In fact, later, our numerical calculations will show that such mechanism can help to eliminate the impact of optical losses caused by the quantum system. In other words, the optical loss of the quantum microsystem is no longer the determining factor in selecting a microsystem for our multiple reflection scheme. Microsystems capable of implement optical path blocking, such as Rydberg blockade [59-61], photon blockade [62], and so on [58,63], are still good candidates to apply our method to achieve CS preparation. Consequently, it doesn't matter whether the experimental quantum microsystem absorbs photons or provides π phase. The real contribution of our scheme is that the microsystem only needs to function properly within a weak field environment. This gives advantage for our scheme to be utilized in any given experimental environment and has the potential for practical application in the future. In the following, we will analyze a detailed experimental scheme based on a specific microscopic system in order to study the performance of our method under realistic conditions.

For illustrative purposes only, we adopt the atom-single side cavity system in Ref. [37] as our quantum microsystem. As shown in Fig.1b, a single atom is embedded in a single-side cavity SSC_1 , which is constituted by two facing mirrors CM_R and CM_T . Ideally, CM_T is assumed to have perfect reflection, but CM_R is allowed for in- and outcoupling of light. The energy level configuration of the atom is shown in the upper right corner of Fig.1b. The transition between levels $|\uparrow\rangle$ and $|e\rangle$ is coupled by the cavity mode. When the atom is in $|\uparrow\rangle$, the weak coherent light pulse, resonant with the cavity, is prevented from entering the cavity due to normal-mode splitting, which results in reflection without a π phase shift. As for the transition between $|\downarrow\rangle$ and $|\uparrow\rangle$, it is decoupled from the cavity mode due to large detuning. Therefore, when the atom is in $|\downarrow\rangle$, the cavity can be treated as an empty cavity. The incident pulse enters the cavity and reflects back but with a π phase. In Refs. [37,42], this atom-cavity coupling model is directly used to generate CS. After a single reflection (Hereinafter we call it the single reflection scheme), the atom-field entanglement

$(|\alpha\rangle|\uparrow\rangle + |-\alpha\rangle|\downarrow\rangle)/\sqrt{2}$ can be generated. Unfortunately, later on, we will explain why the method becomes ineffective when the incident light field is strong. In simple terms, as the external field strengthens, a single atom is ultimately unable to prevent the optical field from entering the cavity. Once the light enters the cavity, the reflected field must carry a π phase shift no matter what the atomic state is, just as in the case of empty cavity reflection. The atom-cavity system is no longer functioning to manipulate the light field, but this problem can be solved by our solution.

Based on the atom-cavity system, our detailed experimental scheme is presented in Fig.1b. In order to implement multiple interactions between the atom and light field, we do not directly use the chain interferometer structure in Fig.1a, but rather its equivalent Michelson interferometer. In the figure, SM stands for switchable mirror (In the experiment, it can be realized by a fiber switch [64] or Pockels cell [65-68]), which is transparent only at the beginning and end of preparation. At all other times, it is just a normal mirror, forcing the light pulse to bounce back and forth inside the interferometer for M cycles. One cycle is defined by a pulse starting at SM , going through BS twice, and returning to SM . Because the optical field passes through the BS twice with each interaction with the atom, we adjust the parameter of BS to $\theta = \pi/2M$. In addition, SSC_0 is an empty single-side cavity. Except for the absence of atom, everything else is the same as SSC_1 . C stands for optical circulator. PS stands for phase shifter. Unlike other components, the use of PS is only for the convenience of calculation and discussion. Its removal does not have a substantial impact on our method. We assume that PS adds a π phase shift to the light field only as it propagates from BS to SSC . Its function can be described as $a_z^\dagger \rightarrow -a_z^\dagger$, where we still set a_z^\dagger ($z = 0,1$) as the creation operator of the light field in Zone z .

Initially, the light source emits a coherent pulse into the interferometer, while the light field in Zone 1 is in a vacuum state. As for the atom, it is prepared in a superposition state. Accordingly, the initial state of the entire system is $|\alpha, 0\rangle(|\uparrow\rangle + |\downarrow\rangle)/\sqrt{2}$. After m number of cycles, the wavefunction of the whole system becomes (See Method A)

$$|\psi^{(2m)}\rangle = \frac{1}{\sqrt{2}}(|\alpha, 0\rangle|\uparrow\rangle + |\alpha \cos 2m\theta_M, \alpha \sin 2m\theta_M\rangle|\downarrow\rangle). \quad (1)$$

The dynamic evolution process of the system can be briefly described as follows. Due to the presence of the empty cavity SSC_0 , when the atom is in $|\downarrow\rangle$, light field has no phase difference in Zones 0 and 1. Interference continues to occur, thereby generating $|-\alpha\rangle$. On the contrary, when the atom is in $|\uparrow\rangle$, the light field is frozen in $|\alpha\rangle$ due to the phase difference between the two Zones. Consequently, after M cycles, we have the light-atom entangled state $(|\alpha, 0\rangle|\uparrow\rangle + |-\alpha, 0\rangle|\downarrow\rangle)/\sqrt{2}$. We note that the light field is output from the SM_0 end and no photons appear at SM_1 side. After measuring the atom, the optical CS is deterministically prepared.

So far, we have only focused on the ideal case. In the following, we analyze the performance of our multiple reflection scheme for non-ideal situation. We show that our scheme is highly durable when it comes to parameters such as atomic spontaneous emission decay and atom-cavity detuning. The reason for this is the quantum Zeno effect caused by light absorption.

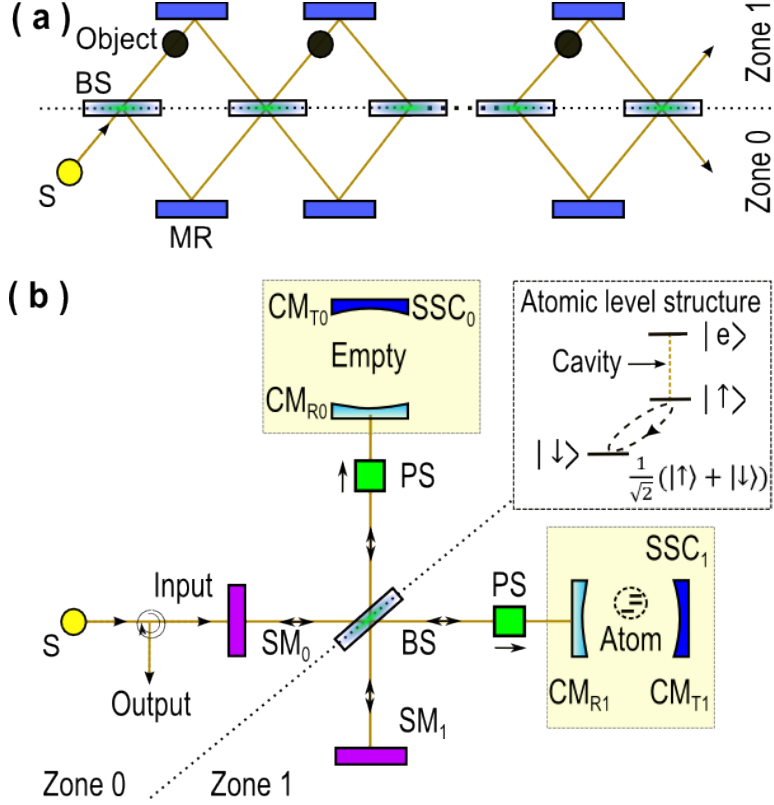


FIG. 1 (a) Principle model based on chain interferometer. (b) Multiple reflection scheme based on a Michelson interferometer. When the switchable mirrors (SM) are turned on, the coherent light pulse is bounced inside the interferometer and interact with the single-side cavity (SSC) for M times. Inside SSC_1 there is an atom whose level structure is shown on the up-right side.

C. Experimental parameter analysis of multiple reflection scheme based on single-side cavity-atom coupling system

In the upcoming discussion, we utilize numerical simulations to analyze the impact of various practical parameters, including atomic, cavity parameters, the number of cycles, and the light loss rates of classical optical devices. We employ fidelity and cattiness [69-71] as metrics to assess the quality of the CS generated by our method. Additionally, recognizing the critical role of light loss in CS preparation [71], we also emphasize the discussion of two types of optical losses. Following the categorization presented in the introduction, the first type is caused by the quantum system, specifically the atom-cavity interaction, while the second type solely originates from classical optical devices.

To begin with, we briefly outline the definitions of each parameter and our numerical simulation method, followed by a detailed discussion of the impact of these parameters. Regarding the practical atom-cavity system (SSC_1), the incident light field is not only reflected, but also transmitted and scattered. To evaluate these effects, we set that 2γ and ω_a as the spontaneous emission decay rate and transition frequency of the atomic transition between $|e\rangle$ and $|\uparrow\rangle$, respectively. The coupling constant between the cavity mode with frequency ω_c and the atomic transition is g . The atom-cavity detuning is $\Delta = \omega_a - \omega_c$. Moreover, we set $\kappa_{R(T)}$ as the cavity field decay rate into the external light field on the $CM_{R(T)}$ side. Considering that the atom

is hardly excited in our scheme, as long as the condition of slowly varying light intensities is satisfied [37,45,72], SSC_1 can be well described by the input-output theory [73,74]. Suppose that $|\alpha_{i,1\uparrow}\rangle$ is the incident coherent light field from CM_{R1} side when the atom is in $|\uparrow\rangle$. The cavity reflection $|\alpha_{R,1\uparrow}\rangle$ satisfies (See Method B)

$$\alpha_{R,1\uparrow} = \left[1 - \frac{2\kappa_R(i\Delta+\gamma)}{\kappa(i\Delta+\gamma)+g^2}\right] \alpha_{i,1\uparrow} = |\eta_{R,1\uparrow}| e^{i\beta_{R,1\uparrow}} \alpha_{i,1\uparrow}, \quad (2)$$

where $\kappa = \kappa_R + \kappa_T$, $|\eta_{R,1\uparrow}|^2$ is the reflectivity and $\beta_{R,1\uparrow}$ describes the phase of the reflection. Similarly, for the transmission of the cavity $|\alpha_{T,1\uparrow}\rangle$, we have

$$\alpha_{T,1\uparrow} = -\frac{2(i\Delta+\gamma)\sqrt{\kappa_T\kappa_R}}{\kappa(i\Delta+\gamma)+g^2} \alpha_{i,1\uparrow}. \quad (3)$$

Regarding the scattering field $|\alpha_{S,1\uparrow}\rangle$ due to the atomic spontaneous emission, we have

$$\alpha_{S,1\uparrow} = \frac{2g\sqrt{\kappa_R\gamma}}{\kappa(i\Delta+\gamma)+g^2} \alpha_{i,1\uparrow}. \quad (4)$$

As for the situation that the atom is in $|\downarrow\rangle$, we still assume that the atom is completely unaffected by the cavity mode due to the large detuning. Therefore, SSC_1 in such case can be treated the same as the empty cavity SSC_0 . By setting $g = 0$ in Eqs. (2)-(4), we can immediately obtain the corresponding reflection and transmission. As for the scattering light field, it is obviously 0.

Before we continue our parameter analysis, let us make some necessary discussions about Eqs. (2)-(4). We note that Eqs. (2)-(4) constitute the mathematical foundation of the single reflection model. From the equations, it seems that the preparation of CS in the single reflection model is unrelated to the intensity of the input light $|\alpha|^2$. This indicates that the single reflection model allows for a certain degree of flexibility in $|\alpha|^2$. However, to derive Eqs. (2)-(4), the weak excitation approximation is required (see Eq. (15) in Method B), meaning that the light field inside the cavity cannot be too strong. This leads to the requirement that the cavity parameter κ_R not be too large, and similarly, the intensity of the incident field or the peak value of the incident pulse must also be constrained. When the peak value of the incident pulse is limited, those of the output CS pulse waveshape is also constrained. How to overcome these limitations is one of the goals that our work aims to solve. When parameters such as κ_R , κ_T , γ , Δ , g and pulse length are fixed, increasing the intensity of the incident light always invalidate Eqs.(2)-(4). To keep the equations valid, further improvement of the system parameters is necessary. By utilizing our scheme, the single-side cavity-atom coupling system can always work under the appropriate external field intensity. This effectively leads to avoid the difficulties brought about by improvement of the quantum system. From this perspective, our method is not a negation of the single reflection method. The core principle of our approach is to enhance and broaden the operational spectrum of the atom-cavity coupling system. The two methods are complementing each other.

Returning to our parameter analysis, based on our previous mathematical description of SSC_0 and SSC_1 , we can numerically simulate the dynamic evolution process of the input coherent pulse $|\alpha\rangle$ and the fidelity of the output. We suppose that the target state is $|\psi_T\rangle = (|\alpha\rangle|\uparrow\rangle + |-\alpha\rangle|\downarrow\rangle)/\sqrt{2}$, and the final state of the whole system after M cycles is $|\psi_f\rangle = (|C_{0\uparrow}\rangle|loss_{\uparrow}\rangle|\uparrow\rangle + |C_{0\downarrow}\rangle|loss_{\downarrow}\rangle|\downarrow\rangle)/\sqrt{2}$ with $|loss_{\uparrow(\downarrow)}\rangle = |C_{1\uparrow(\downarrow)}\rangle \otimes \prod_{m=1}^M \left| \alpha_{T,0\uparrow(\downarrow)}^{(m)} \right| \left| \alpha_{S,0\uparrow(\downarrow)}^{(m)} \right| \left| \alpha_{T,1\uparrow(\downarrow)}^{(m)} \right| \left| \alpha_{S,1\uparrow(\downarrow)}^{(m)} \right|$. Here state $|C_{z\uparrow(\downarrow)}\rangle$ ($z = 0,1$) denotes the outputs appearing at SM_z side when the atom is in state $|\uparrow(\downarrow)\rangle$. $\left| \alpha_{T,z\uparrow(\downarrow)}^{(m)} \right|$ denotes the transmission field

generated by SSC_z in the m -th cycle, while $|\alpha_{S,z\uparrow(\downarrow)}^{(m)}\rangle$ denotes the scattering field. Therefore, $|\text{loss}_{\uparrow(\downarrow)}\rangle$ includes all optical losses caused by the atom-cavity coupling system, while the fidelity is obtained by tracing $|\text{loss}_{\uparrow(\downarrow)}\rangle$, i.e., $F = \text{Tr}_{\text{loss}}\{\langle\psi_T|\psi_f\rangle\langle\psi_f|\psi_T\rangle\} = \{|\langle\alpha|C_{0\uparrow}\rangle|^2 + |\langle-\alpha|C_{0\downarrow}\rangle|^2 + 2\text{Re}[\langle\alpha|C_{0\uparrow}\rangle\langle C_{0\downarrow}|-\alpha\rangle\langle\text{loss}_{\downarrow}|\text{loss}_{\uparrow}\rangle]\}/4$. In addition to fidelity F , in our subsequent analysis, we also investigate cattiness [69-71], $C_a = (|\langle\text{loss}_{\uparrow}|\text{loss}_{\downarrow}\rangle|^2 - |\langle C_{0\uparrow}|C_{0\downarrow}\rangle|^2)|C_{0\uparrow} - C_{0\downarrow}|^2/4$. Detailed calculations can be found in Method C. This physical quantity characterizes the purity of the prepared CS. Its maximum value is equal to $|\alpha|^2$. Apparently, C_a is more sensitive to light loss compared to F , since its value is related to $|\langle\text{loss}_{\downarrow}|\text{loss}_{\uparrow}\rangle|^2$, while F is solely related to $|\langle\text{loss}_{\downarrow}|\text{loss}_{\uparrow}\rangle|$.

As a comparison, we also consider the single reflection model in Ref.[37]. More specifically, the input $|\alpha\rangle$ is directly reflected by SSC_1 , and the corresponding output state is $(|\alpha_{R,1\uparrow}\rangle|\text{loss}_{\uparrow}\rangle|\uparrow\rangle + |\alpha_{R,1\downarrow}\rangle|\text{loss}_{\downarrow}\rangle|\downarrow\rangle)/\sqrt{2}$ with $|\text{loss}_{\uparrow(\downarrow)}\rangle = |\alpha_{T,1\uparrow(\downarrow)}\rangle|\alpha_{S,1\uparrow(\downarrow)}\rangle$. In this model, the constraints on the atomic parameters γ and Δ can be directly obtained from Eq. (2). For the empty cavity case (atom is in $|\downarrow\rangle$), as long as $\kappa_T = 0$, the ideal reflection $\alpha_R = -\alpha_i$ can be obtained. As for the case where the atom is in $|\uparrow\rangle$, the condition for ideal reflection $\alpha_R = \alpha_i$ is $\Delta = \gamma = \kappa_T = 0$. If only γ is non-zero, we can see that the ideal reflection can be approximately achieved only when $\gamma \ll g^2/\kappa_R$. As γ increases, the cavity reflectivity $|\eta_{R,1\uparrow}|^2$ decreases monotonically until it drops to 0 when $\gamma = g^2/\kappa_R$. In other words, γ causes of the first type of light loss. If we focus on Δ , however, it only affects $\beta_{R,1\uparrow}$ when $\gamma = \kappa_T = 0$, since $|\eta_{R,1\uparrow}|^2 = 1$. As Δ varies from $-\infty$ to ∞ , $\beta_{R,1\uparrow}$ decreases monotonically from π to $-\pi$. In order to ensure that $\beta_{R,1\uparrow}$ is close to 0, the constraint $\Delta \ll g^2/\kappa_R$ is required. Our subsequent numerical simulations will demonstrate that satisfying the constraints $\gamma \ll g^2/\kappa_R$ and $\Delta \ll g^2/\kappa_R$ is necessary for the single reflection model to function properly. In our multiple reflection scheme, however, the above constraints are relaxed. In the following, we show that our scheme can become less sensitive to atomic parameters γ and Δ under certain conditions, thus the fidelity of CS depends only on the quality of the classical optical system.

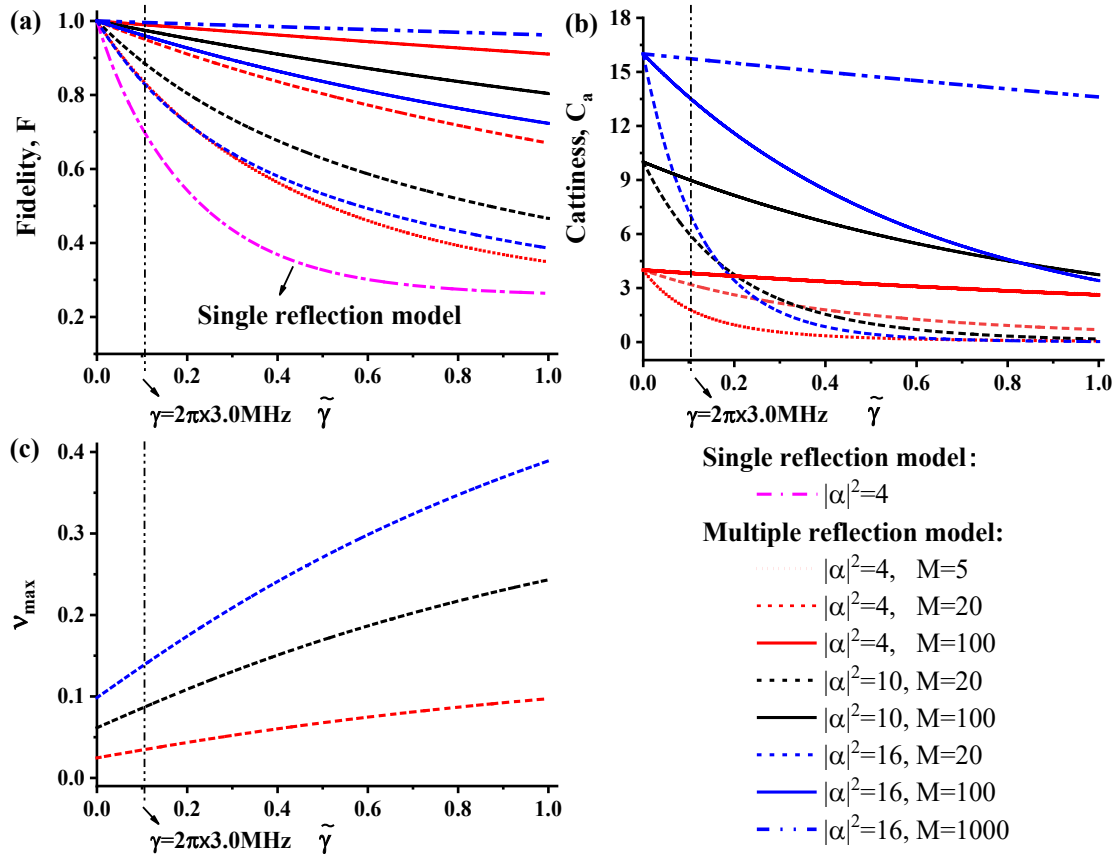


Fig.2 (a) Fidelity F and (b) cattiness C_a versus dimensionless $\tilde{\gamma} = \kappa_R \gamma / g^2$ with $g = 2\pi \times 7.8 \text{ MHz}$, $\kappa_R = \kappa = 2\pi \times 2.3 \text{ MHz}$ and $\Delta = 0$. The pink dotted dashed curve is for the single reflection case. Other curves are for the multiple reflection case. Different colors represent different $|\alpha|^2$. Different styles represent different M . (c) We plot v_{\max} versus $\tilde{\gamma}$ when $M = 20$, where v_{\max} is the maximum value of the average photon number reaching SSC_1 in each cycle when the atom is in $|\uparrow\rangle$.

Effect of atomic spontaneous emission decay rate γ

From the above analysis, it is evident that the atomic parameter γ is the primary source of the first type of light loss. In order to analyze the effect of γ , we plot the fidelity F and cattiness C_a against $\tilde{\gamma} = \kappa_R \gamma / g^2$ with $g = 2\pi \times 7.8 \text{ MHz}$, $\kappa_R = \kappa = 2\pi \times 2.3 \text{ MHz}$ and $\Delta = 0$ in Fig. 2, where $1/\tilde{\gamma}$ is the cooperativity. In this simulation, we assume that all classical optical devices such as SM are ideal. The pink dotted dashed curve is plotted for the single reflection model with $|\alpha|^2 = 4$, which has almost reached the upper limit of such model [37]. The remaining curves illustrate the multiple reflection model. Red curves correspond to $|\alpha|^2 = 4$, black to $|\alpha|^2 = 10$, and blue to $|\alpha|^2 = 16$. Dotted curves are used for $M = 5$, dashed curves for $M = 20$, solid curves for $M = 100$, and double-dotted dashed curves for $M = 1000$. In addition, we plot for v_{\max} in fig.2c when $M = 20$, where $v_{\max} = \max \left\{ \left| \alpha_{i,1\uparrow}^{(1)} \right|^2, \left| \alpha_{i,1\uparrow}^{(2)} \right|^2, \dots, \left| \alpha_{i,1\uparrow}^{(m)} \right|^2 \dots \right\}$ is the maximum value of the average photon number reaching SSC_1 in each cycle when the atom is in $|\uparrow\rangle$. As shown in the figure, v_{\max} is always less than 1 (For other M , the situation is similar), which validates the low atomic excitation probability condition, hence Eqs. (2)-(4) are valid for simulations.

By comparison, we can see that the multiple reflection scheme outperforms the single reflection scheme. In our scheme, it is evident that fidelity increases as M increases. Whereas for larger $|\alpha|^2$, larger M is required to achieve the same fidelity. More importantly, for γ much larger than $2\pi \times 3.0\text{MHz}$ (This value is taken from the experiment in Ref. [37]. It corresponds to $\tilde{\gamma} \approx 0.11$ and has been marked in the figure), our scheme can still provide large F . To better explain the result, we consider the extreme case when $\tilde{\gamma} = 1$, which means all photons reaching SSC_1 in a single cycle are lost when the atom is in $|\uparrow\rangle$. Under such conditions, the interference between Zone 0 and Zone 1 is continuously interrupted, resulting in the output light field state in Zone 0 becomes $|\alpha \cos^2(\pi/2M) \cos^{M-1} 2(\pi/2M)\rangle \approx |\alpha(1 - \pi^2/2M)\rangle$ [48,49], where the approximation is valid when M is sufficiently large. It is evident that when $M \gg |\alpha|$, the output photon state approaches $|\alpha\rangle$, signifying that the total light loss induced by the atom-cavity coupling system over the entire preparation process (M cycles) actually diminishes. This phenomenon is a manifestation of the quantum Zeno effect we previously discussed, which is a consequence of photon loss from individual atom-cavity coupling system. Notably, the cumulative loss is directly proportional to $|\alpha|^2$ and inversely proportional to M . This can explain why in Fig.2a, the larger M and the smaller $|\alpha|^2$, the better the fidelity. So far, our discussion is about $\tilde{\gamma} = 1$. As for the case of $0 < \tilde{\gamma} < 1$, the situation is similar. There is a mixture of two physical mechanisms. The first is to maintain the initial state by phase modulation, which does not cause any photon loss. The second is the quantum Zeno effect, which brings photon loss to the entire system. As $\tilde{\gamma}$ increases, the role of the second mechanism becomes increasingly important. However, by increasing M , the total loss can be greatly suppressed. Therefore, the quantum Zeno effect determines the lower bound of fidelity of our scheme, which is consistent with the simulation in the figure. Together, the above two mechanisms ensure that our scheme has higher fidelity and higher tolerance to γ than the single reflection scheme as M increases. In addition, since the condition $\gamma \ll g^2/\kappa_R$ is relaxed, it implies that our scheme does not require strong coupling between atom and cavity when the value of γ is fixed.

Regarding cattiness, due to its greater sensitivity to light loss, achieving high cattiness requires much smaller light loss than the fidelity case. This necessitates a larger value of M . Consequently, we have plotted the blue double-dotted dashed curve for $|\alpha|^2 = 16, M = 1000$ in Fig.2b. It is evident that even when the light loss in an individual atom-cavity coupling system is 100%, the cattiness can still exceed 10. In fact, as previously discussed, even for significantly large values of $|\alpha|^2$, our scheme can ensure high fidelity and cattiness, provided the condition $M \gg |\alpha|$ is satisfied. This means that Type I loss does not limit the size of CS that our scheme can produce.

Effect of atom-cavity detuning Δ

Following the analysis of γ , we discuss the impact of Δ . We have shown that by interrupting the interference, the transmission of the light field from Zone 0 to Zone 1 can be suppressed. Note that the phase mismatch between the two Zones also interrupts the interference, we expect that our scheme can have high tolerance of Δ as well. In Fig. 3, we plot fidelity F and cattiness C_a against $\tilde{\Delta} = \kappa_R \Delta / g^2$. Solid curves are for $\gamma = 0$. Dashed curves are for $\gamma = 2\pi \times 3.0\text{MHz}$. The values of g, κ_R and κ_T are the same as in Fig. 2. In addition, the pink curves are plotted for the single reflection model with $|\alpha|^2 = 4$. As for the multiple reflection model, the red curves are for $|\alpha|^2 = 4, M = 5$, the black curves are for $|\alpha|^2 = 10, M = 20$ and the blue curves are for $|\alpha|^2 = 16, M = 100$, respectively. As shown in Fig.3, even for large $|\alpha|$, as long as M is large, our scheme

can be less sensitive to Δ . Moreover, since Δ does not induce optical losses, the responses of F and C_a to different M are consistent.

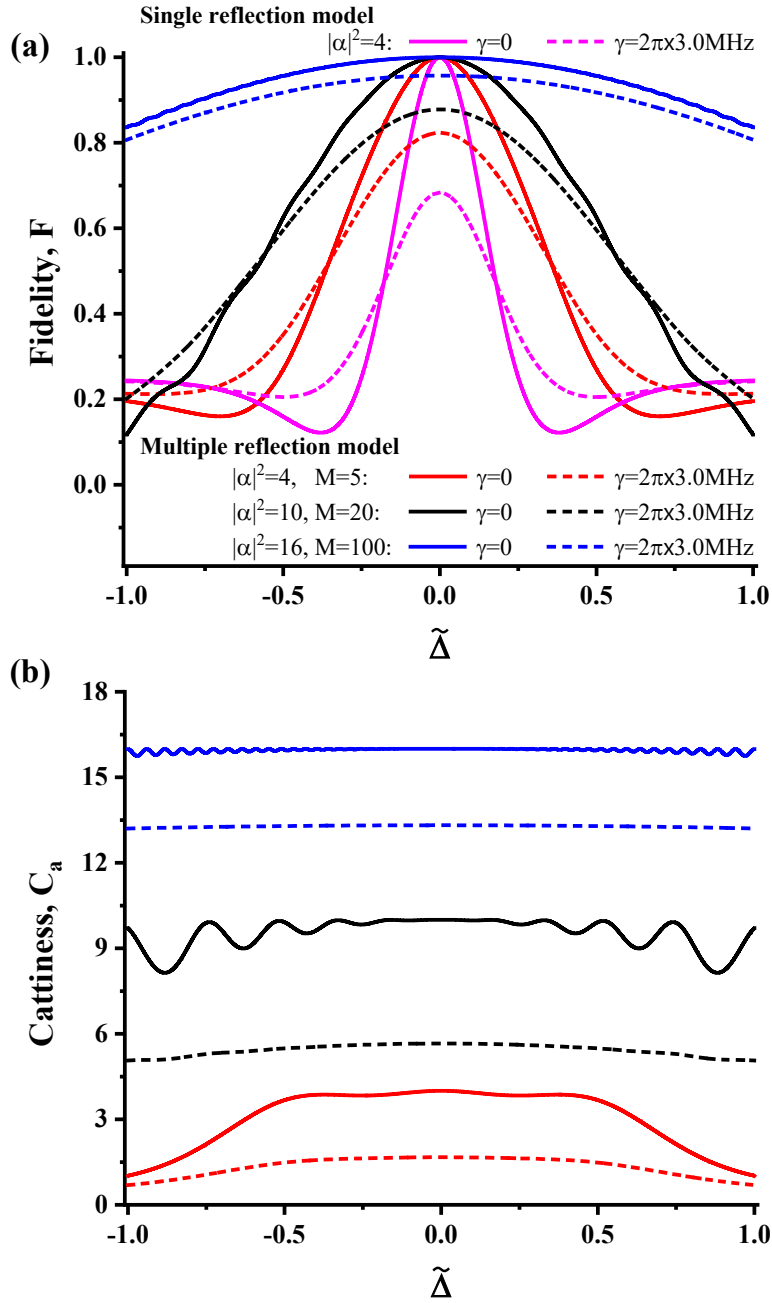


Fig.3 (a) Fidelity F and (b) cattiness C_a versus dimensionless $\tilde{\Delta} = \kappa_R \Delta / g^2$ with $g = 2\pi \times 7.8\text{MHz}$ and $\kappa_R = \kappa = 2\pi \times 2.3\text{MHz}$. The solid curves are for $\gamma = 0$, and dashed curves are for $\gamma = 2\pi \times 3.0\text{MHz}$. The pink curves are for the single reflection model with $|\alpha|^2 = 4$, and other curves are for the multiple reflection scheme.

Effect of the atomic decoherence

Besides the atomic parameters γ and Δ , next we provide a discussion about the influence of the decoherence between the atomic states $|\downarrow\rangle$ and $|\uparrow\rangle$. Obviously, our scheme requires the atom to remain in superposition at least until the end of M cycles. Nevertheless, we need to mention that the multiple reflection processes hardly affect the atomic decoherence. When the atom is in $|\uparrow\rangle$, the low atomic excitation probability can be satisfied. As for the atom in $|\downarrow\rangle$, it is not coupled to the light field. While the atomic superposition state has been reported to last about $400\mu\text{s}$ [75,76]. The full-width at half-maximum of the light pulse that is employed in the experiment of single reflection model is $2.3\mu\text{s}$ [37]. Therefore, it is possible for our scheme to be completed before the decoherence.

Effect of light loss caused by classical optical devices ϵ

So far, we have primarily discussed atomic parameters and optical losses due to atom (Type I loss). Next, we explore the impact of Type II loss, caused by classical optical devices, while keeping Type I light loss constant. We postulate that the loss rate per cycle outside the cavity is denoted by ϵ . Consequently, the cumulative loss rate over the entire preparation process can be approximated as $M\epsilon$, given that $(1 - \epsilon)^M \approx 1 - M\epsilon$ under the assumption of a small ϵ . Furthermore, considering the symmetrical of the optical devices on both arms of the interferometer, it is reasonable to assume that Type II loss is identical for each arm. Consequently, ϵ can be expressed as the sum of the light losses from each optical device located on a single arm of the interferometer. To facilitate our discussion, we assume that all optical devices are ideal, except for the switchable mirror SM (We also assume that irrespective of whether SM is turned on or off, its light loss rate remains constant). Consequently, when coherent light $|\beta_z\rangle$ incident upon SM_z ($z = 0,1$), the reflected field is denoted as $|\sqrt{1 - \epsilon}\beta_z\rangle$, and the lost light field can be represented as $|\sqrt{\epsilon}\beta_z\rangle$. In our simulation, the effect of the term $|\sqrt{\epsilon}\beta_z\rangle$ is accounted for by taking the trace, similar to our treatment of the cavity mentioned earlier.

In Fig.4, we plot ϵ against effective fidelity $F_{ef} = \text{Tr}_{\text{loss}}\{\langle\psi_{ef}|\psi_f\rangle\}$, cattiness C_a , and output intensity $|\alpha_{ef}|^2$ for different $|\alpha|^2$ and M . Here, F_{ef} differs from F in that the target state is set as $|\psi_{ef}\rangle = (|\alpha_{ef}\rangle|\uparrow\rangle + |-\alpha_{ef}\rangle|\downarrow\rangle)/\sqrt{2}$ with $\alpha_{ef} = -C_{0\downarrow} = \alpha [(\kappa_R - \kappa_T)/(\kappa_T + \kappa_R)]^M$. Note that $|C_{0\downarrow}\rangle$ is the output when the atom is in $|\downarrow\rangle$, where interference occurs between the two empty cavities. If the optical parameters of these two cavities are the same, only intensity of the output is affected and reduced from $|\alpha|^2$ to $|\alpha_{ef}|^2$. For the cavity-atom system, the parameters are set as $g = 2\pi \times 7.8\text{MHz}$, $\kappa_R = 2\pi \times 2.3\text{MHz}$, and $\gamma = 2\pi \times 3.0\text{MHz}$, aligning with actual cavity characteristics. However, for κ_T , we set it to zero. Based on the above parameters, the corresponding Type I loss is about 36.6%. Before we begin analyzing the impact of Type II light loss, it is important to note that the role of κ_T can be simulated with ϵ , since the main impact of κ_T is on the empty cavity light loss. This type of loss is categorized as light loss from classical optical devices and can be added to other Type II losses. Therefore, here we simply treat it as 0. Detailed explanations regarding κ_T are provided later.

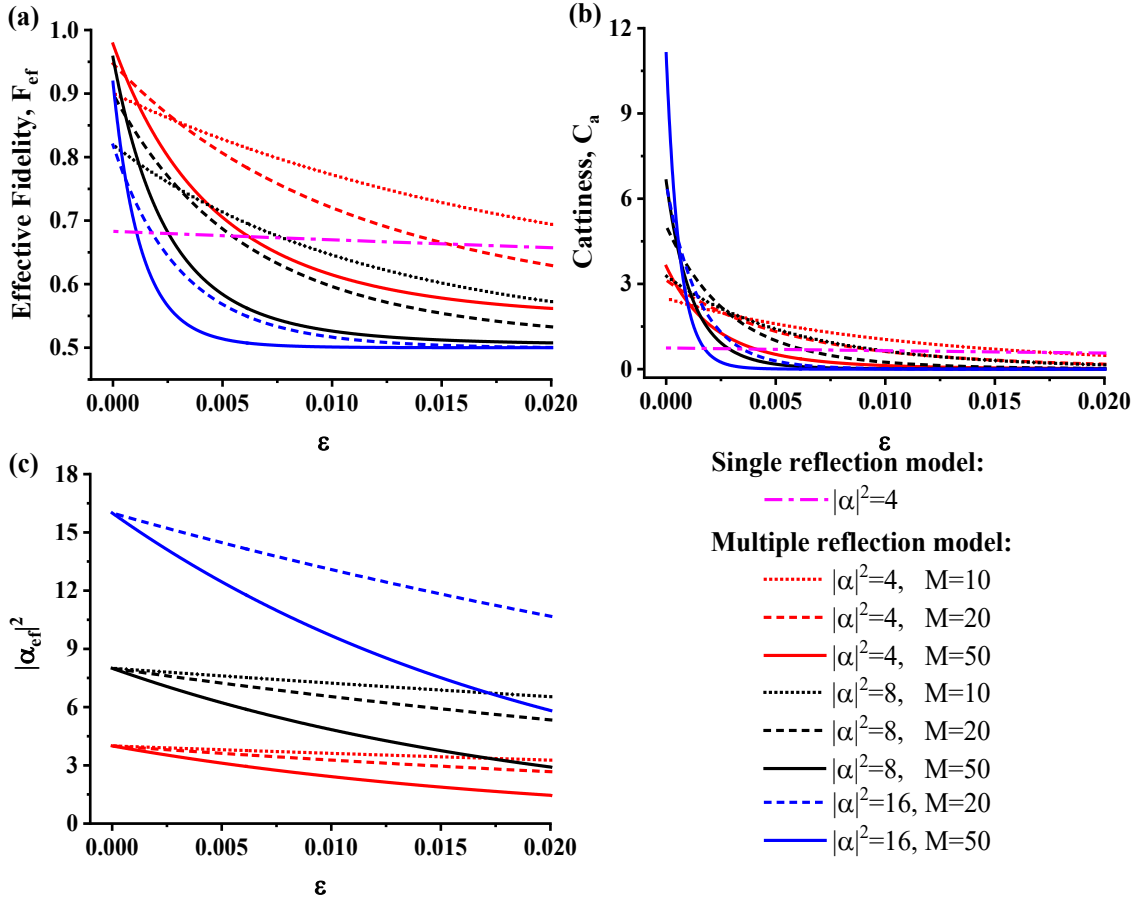


Fig.4 (a) Effective fidelity F_{ef} , (b) cattiness C_a , and (c) the output intensity $|\alpha_{ef}|^2$ versus ϵ with $g = 2\pi \times 7.8\text{MHz}$, $\gamma = 2\pi \times 3.0\text{MHz}$, $\kappa_R = \kappa = 2\pi \times 2.3\text{MHz}$, and $\Delta = 0$. The pink dotted dashed curves are for the single reflection model with $|\alpha|^2 = 4$, and other curves are for the multiple reflection scheme with different $|\alpha|^2$ and M . The target state is $(|\alpha_{ef}\rangle|\uparrow\rangle + |-\alpha_{ef}\rangle|\downarrow\rangle)/\sqrt{2}$.

For comparison, we have also plotted the curves corresponding to the single reflection model at $|\alpha|^2 = 4$ (the pink dotted dashed curves). In this scenario, both F_{ef} and C_a demonstrate minimal impact from ϵ , indicating that the key factor affecting the single reflection model here primarily stems from the optical losses in the individual atom-cavity system. In this context, we utilize this as a baseline to assess the quality of CS preparation in the multiple reflection model. From Fig.4a and 4b, it can be observed that when ϵ is large, the multiple reflection model suffers from Type II light loss across various parameters, with both F_{ef} and C_a falling below that of the single reflection model. As M increases, the situation deteriorates further. However, as ϵ decreases, a dramatic shift occurs. Both F_{ef} and C_a begin to outperform the single reflection case and rapidly increase. Smaller values of $|\alpha|^2$ and M exhibit a higher tolerance to Type II light loss, but larger M values can achieve greater maximal values of F_{ef} and C_a (at $\epsilon = 0$). As a result, there are observable intersections of curves for different M values for a given $|\alpha|^2$, which implies that it's possible to obtain better fidelity using higher M . For larger values of $|\alpha|^2$, such improvements due to M are only noticeable when ϵ is closer to zero. These observed effects are due to the fact that as ϵ approaches zero, the impact of Type I losses gradually becomes dominant, and our

method effectively suppresses the influence of Type I light loss. It's important to recognize that in the single reflection model, Type I light losses are inevitable and can only be reduced through improvements in the atom-cavity system. In contrast, our multiple reflection approach, while not immune to light losses from classical optical devices, offers a novel method to reduce the stringent requirements on quantum microscopic system, including the atom-cavity coupling system, which is used to prepare the CS. This is the central and distinctive feature of our work.

To pave the way for the initiation of proof-of-concept experiments, we also provide two tables below specifying the loss tolerances for classical optical devices in a single cycle. These tolerances are required to achieve certain levels of effective fidelity and cattiness under varying conditions of $|\alpha|^2$ and M . The tables reveal that, to achieve over 70% effective fidelity in conditions with $|\alpha|^2 \leq 4$ and $M \leq 10$, our scheme's tolerance for Type II loss can be close to or even exceed 2%. For larger $|\alpha|^2$, however, our scheme requires much smaller ϵ . Hence, for our scheme, the constraint on preparing large-sized CS is tied to the quality of classical optical devices.

Effective fidelity		$F_{ef} \geq 70\%$	$F_{ef} \geq 80\%$	$F_{ef} \geq 90\%$	$F_{ef} \geq 95\%$
$ \alpha ^2$	M	ϵ	ϵ	ϵ	ϵ
3	6	$\leq 3.9 \times 10^{-2}$ ($ \alpha_{ef} ^2 = 2.36$)	$\leq 1.3 \times 10^{-2}$ ($ \alpha_{ef} ^2 = 2.77$)		
3	10	$\leq 2.9 \times 10^{-2}$ ($ \alpha_{ef} ^2 = 2.24$)	$\leq 1.2 \times 10^{-2}$ ($ \alpha_{ef} ^2 = 2.66$)	1.9×10^{-3} ($ \alpha_{ef} ^2 = 2.94$)	
4	8	$\leq 2.1 \times 10^{-2}$ ($ \alpha_{ef} ^2 = 3.38$)	$\leq 7.3 \times 10^{-3}$ ($ \alpha_{ef} ^2 = 3.77$)		
4	10	$\leq 1.9 \times 10^{-2}$ ($ \alpha_{ef} ^2 = 3.3$)	$\leq 7.4 \times 10^{-3}$ ($ \alpha_{ef} ^2 = 3.71$)	$\leq 2 \times 10^{-5}$ ($ \alpha_{ef} ^2 = 3.98$)	
4	50	$\leq 5.2 \times 10^{-3}$ ($ \alpha_{ef} ^2 = 3.08$)	$\leq 2.5 \times 10^{-3}$ ($ \alpha_{ef} ^2 = 3.53$)	$\leq 9.2 \times 10^{-4}$ ($ \alpha_{ef} ^2 = 3.82$)	$\leq 3.1 \times 10^{-4}$ ($ \alpha_{ef} ^2 = 3.93$)
8	20	$\leq 4.5 \times 10^{-3}$ ($ \alpha_{ef} ^2 = 7.31$)	$\leq 1.8 \times 10^{-3}$ ($ \alpha_{ef} ^2 = 7.72$)		
8	50	$\leq 2.2 \times 10^{-3}$ ($ \alpha_{ef} ^2 = 7.16$)	$\leq 1.1 \times 10^{-3}$ ($ \alpha_{ef} ^2 = 7.57$)	$\leq 3.4 \times 10^{-4}$ ($ \alpha_{ef} ^2 = 7.87$)	$\leq 3.0 \times 10^{-5}$ ($ \alpha_{ef} ^2 = 7.99$)
16	50	$\leq 9.5 \times 10^{-4}$ ($ \alpha_{ef} ^2 = 15.26$)	$\leq 4.2 \times 10^{-4}$ ($ \alpha_{ef} ^2 = 15.68$)	$\leq 6.0 \times 10^{-5}$ ($ \alpha_{ef} ^2 = 15.95$)	

Table.1 The light loss tolerance of classical optical devices in a single cycle required to achieve a specific effective fidelity F_{ef} for various $|\alpha|^2$ and M values. The corresponding output light intensity $|\alpha_{ef}|^2$ is indicated in parentheses. The parameters are $(g, \gamma, \kappa_R) = 2\pi \times (7.8, 3.0, 2.3)MHz$ and $\kappa_T = \Delta = 0$.

Cattiness		$Ca \geq 50\% \alpha ^2$	$Ca \geq 60\% \alpha ^2$	$Ca \geq 70\% \alpha ^2$	$Ca \geq 80\% \alpha ^2$
$ \alpha ^2$	M	ϵ	ϵ	ϵ	ϵ
3	6	$\leq 2.5 \times 10^{-3}$ ($ \alpha_{ef} ^2 = 2.96$)			
3	10	$\leq 4.7 \times 10^{-3}$ ($ \alpha_{ef} ^2 = 2.86$)	$\leq 2.0 \times 10^{-3}$ ($ \alpha_{ef} ^2 = 2.94$)		
4	8	$\leq 1.5 \times 10^{-3}$ ($ \alpha_{ef} ^2 = 3.95$)			
4	10	$\leq 2.4 \times 10^{-3}$ ($ \alpha_{ef} ^2 = 3.90$)	$\leq 4 \times 10^{-4}$ ($ \alpha_{ef} ^2 = 3.98$)		
4	50	$\leq 1.4 \times 10^{-3}$ ($ \alpha_{ef} ^2 = 3.73$)	$\leq 9.3 \times 10^{-4}$ ($ \alpha_{ef} ^2 = 3.82$)	$\leq 5.7 \times 10^{-4}$ ($ \alpha_{ef} ^2 = 3.89$)	$\leq 2.7 \times 10^{-4}$ ($ \alpha_{ef} ^2 = 3.95$)
8	20	$\leq 6.9 \times 10^{-4}$ ($ \alpha_{ef} ^2 = 7.89$)	$\leq 1.5 \times 10^{-4}$ ($ \alpha_{ef} ^2 = 7.98$)		
8	50	$\leq 6.1 \times 10^{-4}$ ($ \alpha_{ef} ^2 = 7.76$)	$\leq 3.9 \times 10^{-4}$ ($ \alpha_{ef} ^2 = 7.85$)	$\leq 2.0 \times 10^{-4}$ ($ \alpha_{ef} ^2 = 7.92$)	$\leq 4.0 \times 10^{-5}$ ($ \alpha_{ef} ^2 = 7.98$)
16	50	$\leq 1.9 \times 10^{-4}$ ($ \alpha_{ef} ^2 = 15.85$)	$\leq 9.0 \times 10^{-5}$ ($ \alpha_{ef} ^2 = 15.93$)		

Table.2 The light loss tolerance of classical optical devices in a single cycle required to achieve a specific cattiness C_a for various $|\alpha|^2$ and M values. The corresponding output light intensity $|\alpha_{ef}|^2$ is indicated in parentheses. The parameters are $(g, \gamma, \kappa_R) = 2\pi \times (7.8, 3.0, 2.3)MHz$ and $\kappa_T = \Delta = 0$.

Discussion on the cavity parameter κ_T and potential approaches to reduce light loss in empty cavity

Next, we provide additional explanation and clarification on the role of κ_T . It is important to note that κ_T causes light loss when the atom is in both $|\uparrow\rangle$ state and $|\downarrow\rangle$ state, thus affecting both the first and second types of light loss. However, when the atom is in $|\uparrow\rangle$, according to Eqs. (3)-(4), and the fact that $g > \gamma \gg \kappa_T$ [37], the loss caused by light field passing through the atom-cavity coupling system (Eq. (3)) is much smaller than the light loss caused by atomic scattering (Eq. (4)). As for Eq. (4), since $\kappa_T \ll \kappa_R$, the influence of κ_T can be neglected. Hence, the Type I light loss due to κ_T is not the primary concern. As for the situation when the atom is in $|\downarrow\rangle$ and does not participate in interaction, the light transmission of the empty cavity falls under Type II light loss. In other words, the effect of κ_T can be accounted for in ϵ . According to Eq. (2), the light loss rate of the empty cavity after a single reflection is $1 - |(\kappa_T - \kappa_R)/(\kappa_T + \kappa_R)|^2$. In Ref. [37], $\kappa_T = 2\pi \times 0.2 MHz$ and $\kappa_R = 2\pi \times 2.3 MHz$, which results in $\epsilon \approx 29\%$ even if other optical devices are ideal, while after a few reflections, almost all photons are lost. Therefore, the cavity employed in Ref. [37] is unfortunately not suitable for our scheme. To reduce the optical losses, one needs either decrease κ_T , or increase κ_R . The latter is simpler in practice. However, although increasing κ_R can reduce the photon loss during the interference of two empty cavities (The atom is in state $|\downarrow\rangle$), it also increases the photon loss in the presence of atom-cavity coupling (The atom is in state $|\uparrow\rangle$). To verify this, we plot effective fidelity F_{ef} against κ_R with $|\alpha|^2 = 8$, $\gamma = 2\pi \times 3.0 MHz$, and $\Delta = 0$ in Fig.5a (for $M = 10$) and 5b (for $M = 50$). Solid curves represent $\kappa_T = 2\pi \times 0.02 MHz$, while dashed curves represent $\kappa_T = 2\pi \times 0.002 MHz$. Particularly, when $\kappa_R = 2\pi \times 2.3 MHz$, the corresponding light loss rate of the empty cavity is approximately 3.4% for $\kappa_T = 2\pi \times 0.02 MHz$ and 0.35% for $\kappa_T = 2\pi \times 0.002 MHz$. In addition, black curves are for $g =$

$2\pi \times 7.8 \text{ MHz}$, red for $g = 2\pi \times 15 \text{ MHz}$, and blue for $g = 2\pi \times 30 \text{ MHz}$. As for Fig.5c and 5d, the pink curves are plotted for $|\alpha_{ef}|^2$, while other color curves are plotted for C_a . We can see that F_{ef} can be significantly improved as κ_T decreases. As for κ_R , when it increases at the beginning, $|\alpha_{ef}|^2$ rapidly rises to its maximum value 8, which causes F_{ef} to increase. Subsequently, photon loss due to atom-cavity coupling plays a major role, resulting in the decrease of F_{ef} . Particularly, we note that for the black solid curve, when F_{ef} starts to decrease, its corresponding $|\alpha_{ef}|^2$ is not close to 8. The reason is that κ_R is approaching to the limit g^2/γ . Under such limit, the photon loss of a single reflection on SSC_1 when the atom is in $|\uparrow\rangle$ is almost 100%. Therefore, we plot for larger g in order to increase the limit so that the corresponding $|\alpha_{ef}|^2$ of maximum F_{ef} can get closer to the maximum value 8, thereby increasing maximum F_{ef} . As shown in the figure, we can see that the maximum value of F_{ef} increases as g increases. Moreover, κ_R maintains wide range of high fidelity (see blue curve). This is because the constraint $g^2 \gg \kappa_R\gamma$ in our scheme is relaxed. However, we must emphasize that the larger g is not necessary for high fidelity. By decreasing κ_T , we can achieve the same purpose. In fact, the motivation of this work is to reduce the influence of the atom, and to show that the performance of our protocol can be improved by just upgrading the classical optical system, such as the parameters κ_T and ϵ .

Regarding M , we only provide a brief explanation here, as it is consistent with our previous analysis. As shown in Fig.5, when κ_R is small, due to significant Type II light loss, the performance of our scheme does indeed decrease with larger M values. However, as κ_R increases, leading to a decrease in Type II light loss, larger M values can finally offer improved F_{ef} and C_a .

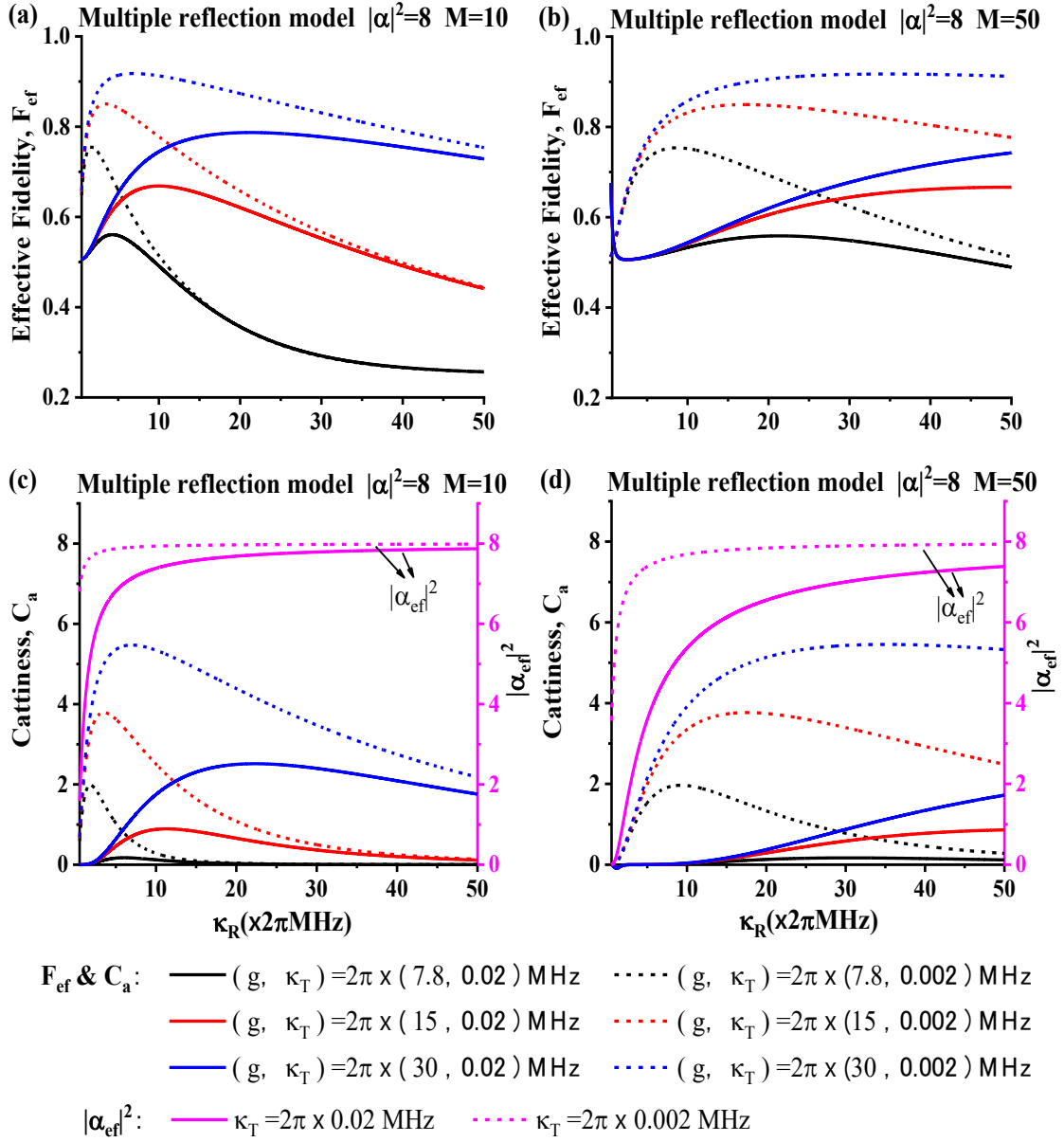


Fig.5 Effective fidelity F_{ef} , cattiness C_a , and the output intensity $|\alpha_{ef}|^2$ versus κ_R with different g , M , and κ_T for the multiple reflection model, where other parameters are $|\alpha|^2 = 8$, $\gamma = 2\pi \times 3.0$ MHz, and $\Delta = 0$. The target state is $(|\alpha_{ef}\rangle|\uparrow\rangle + |-\alpha_{ef}\rangle|\downarrow\rangle)/\sqrt{2}$. Solid curves are for $\kappa_T = 2\pi \times 0.02$ MHz, and dashed curves are for $\kappa_T = 2\pi \times 0.002$ MHz. The pink curves are plotted for $|\alpha_{ef}|^2$ only, while other color curves are plotted for F_{ef} and C_a . Black is for $g = 2\pi \times 7.8$ MHz, red is for $g = 2\pi \times 15$ MHz, and blue is for $g = 2\pi \times 30$ MHz.

Discussion on pulse length and interferometer size

Based on the above analysis of various experimental parameters, we now discuss the requirements of our scheme for the duration of the incident pulse. It is noteworthy that in Ref. [42], the influence of the atom-cavity coupling system on the wave packet waveshape during a

single reflection process has been discussed. The results indicate that to shorten the pulse length by half, while maintaining the reflected waveshape unchanged is necessary to double κ_R . For the single reflection model, an increase in κ_R amplifies Type I losses, resulting in reduced fidelity, hence is not a favorable option. In our scheme, however, since Type I losses can be mitigated, increasing κ_R is feasible. For example, in experiment [37], the pulse duration is $T_p = 2.3\mu s$, and the cavity parameter κ_R is $2\pi \times 2.3MHz$. According to our simulations in Fig. 5, when $|\alpha|^2 = 8$, $M = 50$, $\kappa_T = 2\pi \times 0.002MHz$, and $\kappa_R = 2\pi \times 10MHz$, the effective fidelity of the output CS in our scheme is about 0.75. With κ_R increased by approximately 5 times, the pulse length used in our scheme can be shortened 5 times under the condition of keeping waveshape unchanged, i.e., to $T_p \approx 0.5\mu s$.

We, so far, stipulated that the waveshape of the reflected pulse remains unchanged. This is a requirement from the single reflection model, but not a necessity in our scheme. This is due to the fact that when the atom is in $|\downarrow\rangle$, interference occurs between the two empty cavities, and even if the reflected waveshape distorts, it does not affect the interference process. Conversely, when the atom is in $|\uparrow\rangle$, the role of the atom is merely to disrupt the interference. In this case, the light field is primarily concentrated on the empty cavity side, and the waveshape of the reflected pulse is still determined by the empty cavity reflection. Consequently, variations in the waveshape of the output pulse do not affect the generation of CS. This facilitates further compression of the pulse length in our scheme.

Next, we briefly discuss the size of the interferometer. If we define the size of the interferometer by the distance L between SM_0 and SSC_0 , to ensure that the light-matter interaction in two cycles does not interfere with each other, it implies that L needs to be greater than the half pulse length, i.e., $L \geq (T_p c)/2$, where c is the speed of light. Hence, the total flight distance of the pulse in the entire CS preparation process is $MT_p c$. For a pulse duration $T_p = 2.3\mu s$, L needs to be at least $350m$, and the total flight distance falls within the kilometer scale. Given such distances, employing optical fibers to construct the interferometer is a reasonable choice. Regarding the requirements for light loss from classical optical devices, one can refer to Tables 1 and 2 we previously provided. We note that the parameter κ_R in these tables is specified as $2\pi \times 2.3MHz$. As previously discussed, increasing it allows us to further compress the pulse duration. For instance, setting κ_R to $2\pi \times 10MHz$ results in a pulse duration T_p of $0.5\mu s$, with minimum L adjusted to $75m$. By fixing other parameters at $(g, \gamma) = 2\pi \times (7.8, 3.0)MHz$ and $\kappa_T = \Delta = 0$, along with using $M = 20$ and the best-reported optical fiber, which has an average attenuation of less than $0.157 dB/km$ [77] (the corresponding Type II loss is about 0.53%), the effective fidelity of the output CS is about 0.77 for an input light field of $|\alpha|^2 = 3$. In this estimate, we have not yet accounted for other classical optical losses, such as those from SM and fiber-cavity coupling. If we set these additional losses to 2%, the effective fidelity reduces to 0.63. While our scheme can shift the source of errors from the atomic system to classical optical systems, it also demands higher manufacturing technology standards for existing optical devices.

Lastly, we address the SM . Besides the restrictions brought about by light loss, there are also requirements for its response time T_s . One promising candidate of SM is Pockels cell [65-68]. Applying high voltage, it can rotate the polarization of the light field by 90 degrees, facilitating the extraction of the light field from the interferometer. Its response time is in the nanosecond range. Hence, T_s can be significantly shorter than the duration of the pulse T_p . Strictly speaking, to ensure that the transmission of the pulse is uninterrupted, the length of L should be $(T_p + T_s)c/2$,

which means there needs to be a sufficient time window allowed for the change of state in the Pockels Cell. However, since $T_s \ll T_p$, L is primarily determined by T_p .

III. Conclusion

We propose a macro-micro entanglement generation method based on interaction-free measurement and quantum Zeno effect. Applying our method, optical CS with arbitrarily large average photon number can be prepared deterministically. Due to the fact that in multiple interactions between the quantum microsystem and light field, only a small fraction of photons really interacts with the microsystem, our method allows the quantum microsystem to avoid direct exposure to strong light field, so that the microsystem always works in weak field environment. This indirect controlling mechanism is the key feature of our work. Another feature of our work is its tolerance for photon loss in the quantum microsystem. For illustrative purpose only, we adopt an atom-single side cavity for our quantum microsystem. We show that the state $|- \alpha\rangle$ is generated by multiple optical interferences, which is independent of the quantum microsystem. However, the state $|\alpha\rangle$ comes from the destruction of the interference process, which can be easily achieved even if the quantum microsystem suffers from huge photon loss or other defects such as detuning between the atom and the cavity. This fact allows our scheme to improve the fidelity of the output CS only by perfecting and improving the classical optical system.

IV. Method

A. Calculations for Equation 1

We have mentioned that a_0 and a_1 represent the annihilation operators of the light field in Zone 0 and Zone 1, respectively. Based on this, the function of BS can be described as $a_0^\dagger \rightarrow a_0^\dagger \cos \theta + a_1^\dagger \sin \theta$ and $a_1^\dagger \rightarrow a_1^\dagger \cos \theta - a_0^\dagger \sin \theta$ where $\theta = \pi/2M$. Now, we consider an arbitrary initial photon state

$$|Initial\rangle = |u, v\rangle = \exp(ua_0^\dagger - u^*a_0)\exp(va_1^\dagger - v^*a_1)|0,0\rangle, \quad (5)$$

which represents that a coherent state $|u\rangle$ is in Zone 0 and a coherent state $|v\rangle$ is in Zone 1. After passing through the BS , we have the final state

$$\begin{aligned} |Final\rangle &= \exp[u(a_0^\dagger \cos \theta + a_1^\dagger \sin \theta) - u^*(a_0 \cos \theta + a_1 \sin \theta)], \\ &\quad \times \exp[v(a_1^\dagger \cos \theta - a_0^\dagger \sin \theta) - v^*(a_1 \cos \theta - a_0 \sin \theta)] |0,0\rangle \\ &= |u \cos \theta - v \sin \theta, u \sin \theta + v \cos \theta\rangle. \end{aligned} \quad (6)$$

Similarly, consider an arbitrary phase operation $a^\dagger \rightarrow e^{i\varphi}a^\dagger$. For the initial state $|Initial\rangle = |u\rangle$, after the operation, the final state is

$$\begin{aligned} |Final\rangle &= \exp\left(-\frac{1}{2}|u|^2\right) \sum_{n=0}^{\infty} \frac{u^n}{\sqrt{n!}} \frac{1}{\sqrt{n!}} (e^{i\varphi}a^\dagger)^n |0\rangle \\ &= \exp\left(-\frac{1}{2}|u|^2\right) \sum_{n=0}^{\infty} \frac{1}{\sqrt{n!}} (ue^{i\varphi})^n |n\rangle = |ue^{i\varphi}\rangle \end{aligned} \quad (7)$$

Based on Eqs. (6) and (7), we provide the calculation of Eq. (1).

At the beginning of the preparation, the wave-function of the whole system is

$$|\psi^{(0)}\rangle = \frac{\sqrt{2}}{2} |\alpha, 0\rangle (|\uparrow\rangle + |\downarrow\rangle) \quad (8)$$

In the first cycle, after the photons pass through BS for the first time, the system state is

$$|\psi^{(1)}\rangle = \frac{\sqrt{2}}{2} |\alpha \cos \theta, \alpha \sin \theta\rangle (|\uparrow\rangle + |\downarrow\rangle) \quad (9)$$

Before the photons are reflected by SSC , the system state becomes $\frac{\sqrt{2}}{2} |-\alpha \cos \theta, -\alpha \sin \theta\rangle(|\uparrow\rangle + |\downarrow\rangle)$ due to PS . Regarding the reflection, we emphasize that only when the atom is in $|\uparrow\rangle$, SSC_1 does not change the phase of the reflected field. As a result, the wave function of the whole system becomes $\frac{\sqrt{2}}{2} |\alpha \cos \theta, -\alpha \sin \theta\rangle|\uparrow\rangle + \frac{\sqrt{2}}{2} |\alpha \cos \theta, \alpha \sin \theta\rangle|\downarrow\rangle$. Subsequently, after the second time that the photons pass through BS , we have

$$|\psi^{(2)}\rangle = \frac{\sqrt{2}}{2} |\alpha, 0\rangle|\uparrow\rangle + \frac{\sqrt{2}}{2} |\alpha \cos 2\theta, \alpha \sin 2\theta\rangle|\downarrow\rangle \quad (10)$$

This state becomes the initial state of the second cycle, and the process is repeated. It is not difficult to obtain that after m cycles, the wave-function of the whole system is

$$|\psi^{(2m)}\rangle = \frac{\sqrt{2}}{2} |\alpha, 0\rangle|\uparrow\rangle + \frac{\sqrt{2}}{2} |\alpha \cos 2m\theta, \alpha \sin 2m\theta\rangle|\downarrow\rangle \quad (11)$$

Here the superscript of $|\psi^{(2m)}\rangle$ represents the photons pass through BS $2m$ times.

B. Calculations for Equations 2-4

The Hamiltonian of cavity-atom system (SSC_1) can be described as

$$\begin{aligned} H = & \hbar\omega_e\sigma_{ee} + \hbar\omega_\uparrow\sigma_{\uparrow\uparrow} + \hbar\omega_c a^\dagger a + \hbar \sum_{J=R,T,S} \int_{-\infty}^{\infty} \omega_j b_J^\dagger(\omega_j) b_J(\omega_j) d\omega_j \\ & + \hbar g (\sigma_{\uparrow e} a^\dagger + \sigma_{e\uparrow} a) + \hbar \sqrt{\frac{\gamma}{\pi}} \int_{-\infty}^{\infty} [\sigma_{\uparrow e} b_S^\dagger(\omega_S) + \sigma_{e\uparrow} b_S(\omega_S)] d\omega_S \\ & + i\hbar \sqrt{\frac{\kappa_R}{\pi}} \int_{-\infty}^{\infty} [ab_R^\dagger(\omega_R) - a^\dagger b_R(\omega_R)] d\omega_R + i\hbar \sqrt{\frac{\kappa_T}{\pi}} \int_{-\infty}^{\infty} [ab_T^\dagger(\omega_T) - a^\dagger b_T(\omega_T)] d\omega_T \end{aligned} \quad (12)$$

where $\hbar\omega_e$ is the energy of excited atomic state $|e\rangle$, $\hbar\omega_\uparrow$ is the energy of the atomic state $|\uparrow\rangle$, ω_c is the frequency of the cavity mode described by annihilation operator a , ω_j is the frequency of external field described by annihilation operator $b(\omega_{j=R,T,S})$ with $[b_j(\omega_j), b_j^\dagger(\omega'_j)] = \delta(\omega_j - \omega'_j)$, and the subscript R represents the external multi-mode field on CM_R side, T represents the external field on CM_T side, S represents the scattering field due to the atomic spontaneous emission. In addition, g is coupling constant between the cavity and the atomic transition between $|e\rangle$ and $|\uparrow\rangle$, 2γ is the spontaneous atomic decay rate on the same transition, κ_R and κ_T are cavity field decay rates. We also set that $\sigma_{\uparrow e} = |\uparrow\rangle\langle e|$, $\sigma_{ee} = |e\rangle\langle e|$ and $\sigma_{\uparrow\uparrow} = |\uparrow\rangle\langle\uparrow|$.

Based on the above Hamiltonian, it is not difficult to obtain the following Heisenberg equations

$$\frac{da(t)}{dt} = -i\omega_c a(t) - ig\sigma_{\uparrow e}(t) - \sum_{J=R,T} \sqrt{\frac{\kappa_J}{\pi}} \int_{-\infty}^{\infty} b_J(\omega_J, t) d\omega_J, \quad (13)$$

$$\begin{aligned} \frac{d}{dt} \sigma_{\uparrow e}(t) = & -i(\omega_e - \omega_\uparrow)\sigma_{\uparrow e}(t) + ig[\sigma_{ee}(t) - \sigma_{\uparrow\uparrow}(t)]a(t) \\ & + i\sqrt{\frac{\gamma}{\pi}} \int_{-\infty}^{\infty} [\sigma_{ee}(t) - \sigma_{\uparrow\uparrow}(t)] b_S(\omega_S, t) d\omega_S \\ \approx & -i(\omega_e - \omega_\uparrow)\sigma_{\uparrow e}(t) - iga(t) - i\sqrt{\frac{\gamma}{\pi}} \int_{-\infty}^{\infty} b_S(\omega_S, t) d\omega_S. \end{aligned} \quad (14)$$

In the approximation, we have assumed that [37,45,72]

$$\langle(\sigma_{ee} - \sigma_{\uparrow\uparrow})a\rangle = -\langle a\rangle, \quad (15)$$

which indicates that the atom stays in the state $|\uparrow\rangle$ most of the time. This can be satisfied when the input is weak.

In addition, we can also obtain Heisenberg equations for $b(\omega)$. They are

$$\frac{db_J(\omega_J, t)}{dt} = -i\omega_J b_J(\omega_J, t) + \sqrt{\frac{\kappa_R}{\pi}} a(t), \quad J = R, T, \quad (16)$$

$$\frac{db_S(\omega_S, t)}{dt} = -i\omega_S b_S(\omega_S, t) - i\sqrt{\frac{\gamma}{\pi}}\sigma_{\uparrow e}(t). \quad (17)$$

Eqs. (16) and (17) can be rewritten in integral form. If we assume that the atom-light interaction begins at time $T_{in} < t$, we have

$$b_J(\omega_J, t) = b_J(\omega_J, T_{in})e^{i\omega_J(T_{in}-t)} + \sqrt{\frac{\kappa_J}{\pi}} \int_{T_{in}}^t a(t')e^{i\omega_J(t'-t)} dt', \quad (18)$$

$$b_S(\omega_S, t) = b_S(\omega_S, T_{in})e^{i\omega_S(T_{in}-t)} - i\sqrt{\frac{\gamma}{\pi}} \int_{T_{in}}^t \sigma_{\uparrow e}(t')e^{i\omega_S(t'-t)} dt'. \quad (19)$$

If we assume that the atom-light interaction ends at time $T_{out} > t$, we have

$$b_J(\omega_J, t) = b_J(\omega_J, T_{out})e^{i\omega_J(T_{out}-t)} - \sqrt{\frac{\kappa_J}{\pi}} \int_t^{T_{out}} a(t')e^{i\omega_J(t'-t)} dt', \quad (20)$$

$$b_S(\omega_S, t) = b_S(\omega_S, T_{out})e^{i\omega_S(T_{out}-t)} + i\sqrt{\frac{\gamma}{\pi}} \int_{t_0}^{T_{out}} \sigma_{\uparrow e}(t')e^{i\omega_S(t'-t)} dt'. \quad (21)$$

By integrating Eq. (18) with frequency, it is not difficult to obtain that

$$\begin{aligned} & \sqrt{\frac{\kappa_J}{\pi}} \int_{-\infty}^{\infty} b_J(\omega_J, t) d\omega_J \\ &= \sqrt{\frac{\kappa_J}{\pi}} \int_{-\infty}^{\infty} b_J(\omega_J, T_{in}) e^{i\omega_J(T_{in}-t)} d\omega_J + 2\kappa_J \int_{T_{in}}^t a(t') dt' \frac{1}{2\pi} \int_{-\infty}^{\infty} e^{i\omega_J(t'-t)} d\omega_J \\ &= \sqrt{2\kappa_J} a_{J,in}(t) + \kappa_J a(t). \end{aligned} \quad (22)$$

where we have used the relation [74]

$$\int_{t_0}^t f(t') \delta(t-t') dt' = \int_t^{t_1} f(t') \delta(t-t') dt' = \frac{1}{2} f(t), \quad (t_0 < t < t_1), \quad (23)$$

and the assumptions ($J = R, T$)

$$a_{J,in}(t) = \frac{1}{\sqrt{2\pi}} \int_{-\infty}^{\infty} b_J(\omega_J, T_{in}) e^{i\omega_J(T_{in}-t)} d\omega_J, \quad (24)$$

$$a_{J,out}(t) = \frac{1}{\sqrt{2\pi}} \int_{-\infty}^{\infty} b_J(\omega_J, T_{out}) e^{i\omega_J(T_{out}-t)} d\omega_J. \quad (25)$$

$$a_{S,in}(t) = \frac{1}{\sqrt{2\pi}} \int_{-\infty}^{\infty} b_S(\omega_S, T_{in}) e^{i\omega_S(T_{in}-t)} d\omega_S, \quad (26)$$

$$a_{S,out}(t) = \frac{1}{\sqrt{2\pi}} \int_{-\infty}^{\infty} b_S(\omega_S, T_{out}) e^{i\omega_S(T_{out}-t)} d\omega_S. \quad (27)$$

Similarly, from Eqs. (19)-(21), we have

$$\sqrt{\frac{\gamma}{\pi}} \int_{-\infty}^{\infty} b_S(\omega_S, t) d\omega_S = \sqrt{2\gamma} a_{S,in}(t) - i\gamma \sigma_{\uparrow e}(t), \quad (28)$$

$$\sqrt{\frac{\kappa_J}{\pi}} \int_{-\infty}^{\infty} b_J(\omega_J, t) d\omega_J = \sqrt{2\kappa_J} a_{J,out}(t) - \kappa_J a(t), \quad (29)$$

$$\sqrt{\frac{\gamma}{\pi}} \int_{-\infty}^{\infty} b_S(\omega_S, t) d\omega_S = \sqrt{2\gamma} a_{S,out}(t) + i\gamma \sigma_{\uparrow e}(t). \quad (30)$$

Then, by substituting Eqs. (22)(29) into (13), we can obtain the dynamic equations

$$\frac{da(t)}{dt} = -i\omega_c a(t) - ig\sigma_{\uparrow e}(t) - \sqrt{2\kappa_R} a_{R,in}(t) - \kappa_R a(t) - \sqrt{2\kappa_T} a_{T,in}(t) - \kappa_T a(t), \quad (31)$$

$$\frac{da(t)}{dt} = -i\omega_c a(t) - ig\sigma_{\uparrow e}(t) - \sqrt{2\kappa_R} a_{R,out}(t) + \kappa_R a(t) - \sqrt{2\kappa_T} a_{T,in}(t) - \kappa_T a(t), \quad (32)$$

$$\frac{da(t)}{dt} = -i\omega_c a(t) - ig\sigma_{\uparrow e}(t) - \sqrt{2\kappa_R} a_{R,in}(t) - \kappa_R a(t) - \sqrt{2\kappa_T} a_{T,out}(t) + \kappa_T a(t). \quad (33)$$

By substituting Eqs. (28)(30) into (14), we have

$$\frac{d}{dt} \sigma_{\uparrow e}(t) = -i(\omega_e - \omega_{\uparrow}) \sigma_{\uparrow e}(t) - ig a(t) - i\sqrt{2\gamma} a_{S,in}(t) - \gamma \sigma_{\uparrow e}(t), \quad (34)$$

$$\frac{d}{dt} \sigma_{\uparrow e}(t) = -i(\omega_e - \omega_{\uparrow}) \sigma_{\uparrow e}(t) - ig a(t) - i\sqrt{2\gamma} a_{S,out}(t) + \gamma \sigma_{\uparrow e}(t). \quad (35)$$

In the following, we assume that only the input on CM_R side is none-zero, i.e., $a_{T,in}(t) = a_{S,in}(t) = 0$. Then, by subtracting (31) and (32), we can get the relation between the input $a_{R,in}(t)$ and output $a_{R,out}(t)$,

$$a_{R,in}(t) + \sqrt{2\kappa_R}a(t) = a_{R,out}(t). \quad (36)$$

By subtracting (31) and (33), we have

$$a_{T,out}(t) = \sqrt{2\kappa_T}a(t). \quad (37)$$

By subtracting (34) and (35), we have

$$a_{S,out}(t) = -i\sqrt{2\gamma}\sigma_{\uparrow e}(t). \quad (38)$$

In addition to the above relations, we next calculate the steady-state solution of the dynamic equations (31)(32)(34) by assuming that the cavity-atom system is driven by the input light field with frequency ω . We suppose that

$$\begin{aligned} a_{R,in}(t) &= \alpha_{i,1\uparrow}e^{-i\omega t}, \\ a(t) &= \alpha e^{-i\omega t}, \\ \sigma_{\uparrow e}(t) &= \tilde{\sigma}e^{-i\omega t}, \\ a_{R,out}(t) &= \alpha_{R,1\uparrow}e^{-i\omega t}, \\ a_{T,out}(t) &= \alpha_{T,1\uparrow}e^{-i\omega t}, \\ a_{S,out}(t) &= \alpha_{S,1\uparrow}e^{-i\omega t}. \end{aligned} \quad (39)$$

Then, we can obtain that

$$[-i(\omega_c - \omega) - \kappa_R - \kappa_T]\alpha - ig\tilde{\sigma} - \sqrt{2\kappa_R}\alpha_{i,1\uparrow} = 0, \quad (40)$$

$$[-i(\omega_c - \omega) + \kappa_R - \kappa_T]\alpha - ig\tilde{\sigma} - \sqrt{2\kappa_R}\alpha_{R,1\uparrow} = 0, \quad (41)$$

$$[-i(\omega_e - \omega_{\uparrow} - \omega) - \gamma]\tilde{\sigma} - ig\alpha = 0. \quad (42)$$

It is not difficult to get that

$$\alpha_{i,1\uparrow} = -\frac{[i(\omega_c - \omega) + \kappa_R + \kappa_T][i(\omega_e - \omega_{\uparrow} - \omega) + \gamma] + g^2}{\sqrt{2\kappa_R}[i(\omega_e - \omega_{\uparrow} - \omega) + \gamma]} \alpha, \quad (43)$$

$$\alpha_{R,1\uparrow} = -\frac{[i(\omega_c - \omega) - \kappa_R + \kappa_T][i(\omega_e - \omega_{\uparrow} - \omega) + \gamma] + g^2}{\sqrt{2\kappa_R}[i(\omega_e - \omega_{\uparrow} - \omega) + \gamma]} \alpha. \quad (44)$$

Eq. (43) shows that when the input increases, the intensity of the cavity field also increase, resulting in the condition Eq. (15) not being satisfied.

With Eqs. (43) and (44), we can calculate Eq. (2). Suppose that the cavity and the external field are resonant, i.e., $\omega = \omega_c$, and $\Delta = \omega_e - \omega_{\uparrow} - \omega_c$, we obtain

$$\frac{\alpha_{R,1\uparrow}}{\alpha_{i,1\uparrow}} = 1 - \frac{2\kappa_R(i\Delta + \gamma)}{(\kappa_R + \kappa_T)(i\Delta + \gamma) + g^2}. \quad (45)$$

By using Eqs. (37) and (38), we can also have Eqs. (3) and (4), which are

$$\frac{\alpha_{T,1\uparrow}}{\alpha_{i,1\uparrow}} = -\frac{2\sqrt{\kappa_R\kappa_T}(i\Delta + \gamma)}{(\kappa_R + \kappa_T)(i\Delta + \gamma) + g^2}, \quad (46)$$

$$\frac{\alpha_{S,1\uparrow}}{\alpha_{i,1\uparrow}} = \frac{2\sqrt{\kappa_R\gamma}g}{(\kappa_R + \kappa_T)(i\Delta + \gamma) + g^2}. \quad (47)$$

C. Calculations for Cattiness

Taking into account all possible light losses, the final state of the system after M cycles can be expressed as $|\psi_f\rangle = \frac{1}{\sqrt{2}}(|C_{0\uparrow}\rangle|loss_{\uparrow}\rangle|\uparrow\rangle + |C_{0\downarrow}\rangle|loss_{\downarrow}\rangle|\downarrow\rangle) = \frac{1}{\sqrt{2}}\left[\frac{1}{\sqrt{2}}(|\uparrow\rangle + |\downarrow\rangle)|\psi_0\rangle + \frac{1}{\sqrt{2}}(|\uparrow\rangle - |\downarrow\rangle)|\psi_1\rangle\right]$. After measuring the atom, the light field collapses to state $|\psi_{c=0,1}\rangle = \frac{1}{\sqrt{2}}(|C_{0\uparrow}\rangle|loss_{\uparrow}\rangle + (-1)^c|C_{0\downarrow}\rangle|loss_{\downarrow}\rangle)$ with equal probability. Its corresponding density matrix is

denoted as $|\psi_c\rangle\langle\psi_c|$. By tracing over the loss terms, the resulting reduced density matrix is obtained, represented as

$$\begin{aligned} \rho = Tr_{loss}\{|\psi_c\rangle\langle\psi_c|\} &= \frac{1}{2}|C_{0\uparrow}\rangle\langle C_{0\uparrow}| + \frac{1}{2}|C_{0\downarrow}\rangle\langle C_{0\downarrow}| \\ &+ (-1)^c \frac{1}{2}\langle loss_{\downarrow}|loss_{\uparrow}\rangle|C_{0\uparrow}\rangle\langle C_{0\downarrow}| + (-1)^c \frac{1}{2}\langle loss_{\uparrow}|loss_{\downarrow}\rangle|C_{0\downarrow}\rangle\langle C_{0\uparrow}| \end{aligned} \quad (48)$$

By substituting ρ into the definition of cattiness [69-71]

$$C_a = -Tr[\rho \cdot L(\rho)] \quad (49)$$

with $L(\rho) = a\rho a^+ - \frac{1}{2}\rho a^+ a - \frac{1}{2}a^+ a\rho$, we can obtain that

$$C_a = -\sum_{v=0}^{\infty}\langle v|\rho a\rho a^+|v\rangle + \sum_{v=0}^{\infty}v\langle v|\rho^2|v\rangle \quad (50)$$

where $|v\rangle$ represents Fock state. Utilizing the following expressions ($j = \uparrow, \downarrow$),

$$\langle v|C_{0j}\rangle = \langle v|e^{-\frac{|c_{0j}|^2}{2}}\sum_{u=0}^{\infty}\frac{c_{0j}^u}{\sqrt{u!}}|u\rangle = e^{-\frac{|c_{0j}|^2}{2}}\frac{c_{0j}^v}{\sqrt{v!}} \quad (51)$$

we have

$$C_a = \frac{1}{4}(|\langle loss_{\uparrow}|loss_{\downarrow}\rangle|^2 - |\langle C_{0\uparrow}|C_{0\downarrow}\rangle|^2)|C_{0\uparrow} - C_{0\downarrow}|^2 \quad (52)$$

For comparison, we also give the expression for fidelity here, which is

$$F = \frac{1}{4}\{|\langle\alpha|C_{0\uparrow}\rangle|^2 + |(-\alpha)|C_{0\downarrow}\rangle|^2 + 2\text{Re}[\langle\alpha|C_{0\uparrow}\rangle\langle C_{0\downarrow}|-\alpha\rangle\langle loss_{\downarrow}|loss_{\uparrow}\rangle]\} \quad (53)$$

It can be easily seen that the fidelity is related to $|\langle loss_{\uparrow}|loss_{\downarrow}\rangle|$, while the cattiness is related to $|\langle loss_{\uparrow}|loss_{\downarrow}\rangle|^2$, and thus is more sensitive to light loss.

Reference:

- [1] E. Schrödinger, "Die gegenwärtige Situation in der Quantenmechanik", *Naturwissenschaften* **23**, 807 (1935).
- [2] S. Haroche, "Nobel Lecture: Controlling photons in a box and exploring the quantum to classical boundary", *Rev. Mod. Phys.* **85**, 1083 (2013).
- [3] D. J. Wineland, "Nobel Lecture: Superposition, entanglement, and raising Schrödinger's cat", *Rev. Mod. Phys.* **85**, 1103 (2013).
- [4] L. Li, C.-L. Zou, V. V. Albert, S. Muralidharan, S. M. Girvin, and L. Jiang, "Cat codes with optimal decoherence suppression for a lossy bosonic channel", *Phys. Rev. Lett.* **119**, 030502 (2017).
- [5] S.-W. Lee, and H. Jeong, "Near-deterministic quantum teleportation and resource efficient quantum computation using linear optics and hybrid qubits", *Phys. Rev. A* **87**, 022326 (2013).
- [6] N. Sangouard, C. Simon, N. Gisin, J. Laurat, R. Tualle-Brouiri, and P. Grangier, "Quantum repeaters with entangled coherent states", *J. Opt. Soc. Am. B* **27**, A137 (2010).
- [7] J. B. Brask, I. Rigas, E. S. Polzik, U. L. Andersen, and A. S. Sørensen, "Hybrid long distance entanglement distribution protocol", *Phys. Rev. Lett.* **105**, 160501 (2010).
- [8] H. Jeong and M. S. Kim, "Efficient quantum computation using coherent states", *Phys. Rev. A* **65**, 042305 (2002).
- [9] T. C. Ralph, A. Gilchrist, G. J. Milburn, W. J. Munro, and S. Glancy, "Quantum computation with optical coherent states", *Phys. Rev. A* **68**, 042319 (2003).
- [10] A. P. Lund, T. C. Ralph, and H. L. Haselgrove, "Fault-tolerant linear optical quantum computing with small-amplitude coherent states", *Phys. Rev. Lett.* **100**, 030503 (2008).
- [11] M. Mirrahimi, Z. Leghtas, V. V. Albert, S. Touzard, R. J. Schoelkopf, L. Jiang, and M. H. Devoret, "Dynamically protected cat-qubits: a new paradigm for universal quantum computation", *New Journal of Physics* **16**, 045014 (2014).

- [12] D. Su, I. Dhand, and T. C. Ralph, “Universal quantum computation with optical four-component cat qubits”, *Phys. Rev. A* **106**, 042614 (2022).
- [13] J. Hastrup and U. L. Andersen, “All-optical cat-code quantum error correction”, *Phys. Rev. Research* **4**, 043065 (2022).
- [14] P. T. Cochrane, G. J. Milburn, and W. J. Munro, “Macroscopically distinct quantum-superposition states as a bosonic code for amplitude damping”, *Phys. Rev. A* **59**, 2631 (1999).
- [15] Z. Leghtas, G. Kirchmair, B. Vlastakis, R. J. Schoelkopf, M. H. Devoret, and M. Mirrahimi, “Hardware-efficient autonomous quantum memory protection”, *Phys. Rev. Lett.* **111**, 120501 (2013).
- [16] M. Bergmann and P. van Loock, “Quantum error correction against photon loss using multicomponent cat states”, *Phys. Rev. A* **94**, 042332 (2016).
- [17] N. Ofek, A. Petrenko, R. Heeres, P. Reinhold, Z. Leghtas, B. Vlastakis, Y. Liu, L. Frunzio, S. M. Girvin, L. Jiang, M. Mirrahimi, M. H. Devoret, and R. J. Schoelkopf, “Extending the lifetime of a quantum bit with error correction in superconducting circuits”, *Nature* **536**, 441 (2016).
- [18] W. J. Munro, K. Nemoto, G. J. Milburn, and S. L. Braunstein, “Weak-force detection with superposed coherent states”, *Phys. Rev. A* **66**, 023819 (2002).
- [19] A. Gilchrist, K. Nemoto, W. J. Munro, T. C. Ralph, S. Glancy, S. L. Braunstein, and G. J. Milburn, “Schrödinger cats and their power for quantum information processing”, *J. Opt. B* **6**, S828 (2004).
- [20] J. Joo, W. J. Munro, and T. P. Spiller, “Quantum metrology with entangled coherent states”, *Phys. Rev. Lett.* **107**, 083601 (2011).
- [21] Y. M. Zhang, X. W. Li, W. Yang, and G. R. Jin, “Quantum Fisher information of entangled coherent states in the presence of photon loss”, *Phys. Rev. A* **88**, 043832 (2013).
- [22] S. Ghosh, R. Sharma, U. Roy, and P. K. Panigrahi, “Mesoscopic quantum superposition of the generalized cat state: A diffraction limit”, *Phys. Rev. A* **92**, 053819 (2015).
- [23] A. Facon, E.-K. Dietsche, D. Grosso, S. Haroche, J.-M. Raimond, M. Brune, and S. Gleyzes, “A sensitive electrometer based on a Rydberg atom in a Schrödinger-cat state”, *Nature* **535**, 262–265 (2016).
- [24] E. Polino, M. Valeri, N. Spagnolo, and F. Sciarrino, “Photonic quantum metrology”, *AVS Quantum Science* **2**, 024703 (2020).
- [25] C. Monroe, D. Meekhof, B. King, and D. J. Wineland, “A “Schrödinger cat” superposition state of an atom”, *Science* **272**, 1131 (1996).
- [26] D. Kienzler, C. Flühmann, V. Negnevitsky, H.-Y. Lo, M. Marinelli, D. Nadlinger, and J. P. Home, “Observation of quantum interference between separated mechanical oscillator wave packets”, *Phys. Rev. Lett.* **116**, 140402 (2016).
- [27] S. Deleglise, I. Dotsenko, C. Sayrin, J. Bernu, M. Brune, J.-M. Raimond, and S. Haroche, “Reconstruction of non-classical cavity field states with snapshots of their decoherence”, *Nature* **455**, 510 (2008).
- [28] B. Vlastakis, G. Kirchmair, Z. Leghtas, S. E. Nigg, L. Frunzio, S. M. Girvin, M. Mirrahimi, M. H. Devoret, and R. J. Schoelkopf, “Deterministically encoding quantum information using 100-photon Schrödinger cat states”, *Science* **342**, 607 (2013).
- [29] J. S. Neergaard-Nielsen, B. M. Nielsen, C. Hettich, K. Mølmer, and E. S. Polzik, “Generation of a superposition of odd photon number states for quantum information networks”, *Phys. Rev. Lett.* **97**, 083604 (2006).

- [30] A. Ourjoumtsev, R. Tualle-Brouri, J. Laurat, and P. Grangier, "Generating optical Schrödinger kittens for quantum information processing", *Science* **312**, 83 (2006).
- [31] T. Gerrits, S. Glancy, T. S. Clement, B. Calkins, A. E. Lita, A. J. Miller, A. L. Migdall, S. W. Nam, R. P. Mirin, and E. Knill, "Generation of optical coherent-state superpositions by number-resolved photon subtraction from the squeezed vacuum", *Phys. Rev. A* **82**, 031802(R) (2010).
- [32] H. Takahashi, K. Wakui, S. Suzuki, M. Takeoka, K. Hayasaka, A. Furusawa, and M. Sasaki, "Generation of Large-Amplitude Coherent-State Superposition Via Ancilla-Assisted Photon Subtraction", *Phys. Rev. Lett.* **101**, 233605 (2008).
- [33] K. Huang, H. Le Jeannic, J. Ruaudel, V. B. Verma, M. D. Shaw, F. Marsili, S.W. Nam, E Wu, H. Zeng, Y.-C. Jeong, R. Filip, O. Morin, and J. Laurat, "Optical Synthesis of Large-Amplitude Squeezed Coherent-State Superpositions with Minimal Resources", *Phys. Rev. Lett.* **115**, 023602 (2015).
- [34] A. Ourjoumtsev, H. Jeong, R. Tualle-Brouri, and P. Grangier, "Generation of optical 'Schrödinger cats' from photon number states", *Nature (London)* **448**, 784 (2007).
- [35] A. E. Ulanov, I. A. Fedorov, D. Sychev, P. Grangier, and A. I. Lvovsky, "Loss-tolerant state engineering for quantum enhanced metrology via the reverse Hong-Ou-Mandel effect", *Nat. Commun.* **7**, 11925 (2016).
- [36] D. V. Sychev, A. E. Ulanov, A. A. Pushkina, M. W. Richards, I. A. Fedorov, and A. I. Lvovsky, "Enlargement of optical Schrödinger's cat states", *Nature Photonics* **11**, 379 (2017).
- [37] B. Hacker, S. Welte, S. Daiss, A. Shaikat, S. Ritter, L. Li, and G. Rempe, "Deterministic creation of entangled atom–light Schrödinger-cat states", *Nature Photonics* **13**, 110 (2019).
- [38] M. Dakna, T. Anhut, T. Opatrný, L. Knöll, and D.-G. Welsch, "Generating Schrödinger-cat-like states by means of conditional measurements on a beam splitter", *Phys. Rev. A* **55**, 3184 (1997).
- [39] K. Takase, J.-i. Yoshikawa, W. Asavanant, M. Endo, and A. Furusawa, "Generation of optical Schrödinger cat states by generalized photon subtraction", *Phys. Rev. A* **103**, 013710 (2021).
- [40] A. P. Lund, H. Jeong, T. C. Ralph, and M. S. Kim, "Conditional production of superpositions of coherent states with inefficient photon detection", *Phys. Rev. A* **70**, 020101(R) (2004).
- [41] A. Laghaout, J. S. Neergaard-Nielsen, I. Rigas, C. Kragh, A. Tipsmark, and U. L. Andersen, "Amplification of realistic Schrödinger-cat-state-like states by homodyne heralding", *Phys. Rev. A* **87**, 043826 (2013).
- [42] B. Wang and L.-M. Duan, "Engineering superpositions of coherent states in coherent optical pulses through cavity-assisted interaction", *Phys. Rev. A* **72**, 022320 (2005).
- [43] A. Reiserer, S. Ritter, and G. Rempe, "Nondestructive Detection of an Optical Photon", *Science* **342**, 1349 (2013).
- [44] L.-M. Duan, and H. J. Kimble, "Scalable Photonic Quantum Computation through Cavity-Assisted Interactions", *Phys. Rev. Lett.* **92**, 127902 (2004).
- [45] A. Reiserer, and G. Rempe, "Cavity- based quantum networks with single atoms and optical photons", *Rev. Mod. Phys.* **87**, 1379 (2015).
- [46] M. Mirrahimi, "Cat-qubits for quantum computation", *C. R. Physique* **17**, 778 (2016).
- [47] P. G. Kwiat, H. Weinfurter, T. Herzog, A. Zeilinger, and M. A. Kasevich, "Interaction-free measurement", *Phys. Rev. Lett.* **74**, 4763 (1995).
- [48] H. Salih, Z.-H. Li, M. Al-Amri, and M. S. Zubairy, "Protocol for direct counterfactual quantum communication", *Phys. Rev. Lett.* **110**, 170502 (2013).
- [49] Z.-H. Li, S.-Y. Feng, M. Al-Amri, and M. S. Zubairy, "Direct counterfactual quantum communication protocol beyond single photon source", *Phys. Rev. A* **106**, 032610 (2022).

- [50] Z. L. Wang, Z. H. Bao, Y. K. Wu, Y. Li, W. Z. Cai, W. T. Wang, Y. W. Ma, T. Q. Cai, X. Y. Han, J. H. Wang, Y. P. Song, L. Y. Sun, H. Y. Zhang, L. M. Duan, "A flying Schrödinger's cat in multipartite entangled states", *Sci. Adv.* **8**, eabn1778 (2022).
- [51] Z. H. Bao, Z. L. Wang, Y. K. Wu, Y. Li, W. Z. Cai, W. T. Wang, Y. W. Ma, T. Q. Cai, X. Y. Han, J. H. Wang, Y. P. Song, L. Y. Sun, H. Y. Zhang, and L. M. Duan, "Experimental preparation of generalized cat states for itinerant microwave photons", *Phys. Rev. A* **105**, 063717 (2022).
- [52] X.-S. Ma, X. Guo, C. Schuck, K. Y. Fong, L. Jiang, and H X. Tang, "On-chip interaction-free measurements via the quantum Zeno effect", *Phys. Rev. A* **90**, 042109 (2014).
- [53] Y. Cao, Y.-H. Li, Z. Cao, J. Yin, Y.-A. Chen, H.-L. Yin, T.-Y. Chen, X. Ma, C.-Z. Peng, and J.-W. Pan, "Direct counterfactual communication via quantum Zeno effect", *Proc. Natl. Acad. Sci.* **114**, 4920 (2017).
- [54] C. Liu, J. Liu, J. Zhang, and S.-Y. Zhu, "The experimental demonstration of high efficiency interaction-free measurement for quantum counterfactual-like communication", *Sci. Rep.* **7**, 10875 (2017).
- [55] C. Liu, X. Yang, L. Cui, S. Zhou, and J. Zhang, "Accurate measurement method for refractive index in a high efficiency interaction-free measurement system", *Opt. Express* **28**, 21916 (2020).
- [56] Z.-H. Li, L.-J. Wang, J.-P. Xu, Y.-P. Yang, M. Al-Amri, and M. S. Zubairy, "Counterfactual Trojan horse attack", *Phys. Rev. A* **101**, 022336 (2020).
- [57] J. R. Hance, and J. Rarity, "Counterfactual ghost imaging", *npj Quantum Information* **7**, 88 (2021).
- [58] M. O. Scully and M. S. Zubairy, *Quantum Optics* (Cambridge University Press, Cambridge, 1997).
- [59] E. Urban, T. A. Johnson, T. Henage, L. Isenhower, D. D. Yavuz, T. G. Walker, and M. Saffman, "Observation of Rydberg blockade between two atoms", *Nat. Phys.* **5**, 110 (2009).
- [60] T. A. Johnson, E. Urban, T. Henage, L. Isenhower, D. D. Yavuz, T. G. Walker, and M. Saffman, "Rabi Oscillations between Ground and Rydberg States with Dipole-Dipole Atomic Interactions", *Phys. Rev. Lett.* **100**, 113003 (2008).
- [61] Q. Guo, L. Y. Cheng, L. Chen, H. F. Wang, and S. Zhang, "Counterfactual quantum-information transfer without transmitting any physical particles", *Sci. Rep.* **5**, 8416 (2015).
- [62] K. M. Birnbaum, A. Boca, R. Miller, A. D. Boozer, T. E. Northup, and H. J. Kimble, "Photon blockade in an optical cavity with one trapped atom", *Nature (London)* **436**, 87 (2005)
- [63] G. Nogues, A. Rauschenbeutel, S. Osnaghi, M. Brune, J. M. Raimond, and S. Haroche, "Seeing a single photon without destroying it", *Nature (London)* **400**, 239 (1999).
- [64] Y. Liu, L. Ju, X.-L. Liang, S.-B. Tang, G.-L. Shen Tu, L. Zhou, C.-Z. Peng, K. Chen, T.-Y. Chen, Z.-B. Chen, and J.-W. Pan, "Experimental Demonstration of Counterfactual Quantum Communication", *Phys. Rev. Lett.* **109**, 030501 (2012).
- [65] P. G. Kwiat, A. G. White, J. R. Mitchell, O. Nairz, G. Weihs, H. Weinfurter, and A. Zeilinger, "High-efficiency quantum interrogation measurements via the quantum Zeno effect", *Phys. Rev. Lett.* **83**, 4725 (1999).
- [66] A. I. Bishop and P. F. Barker, "Subnanosecond pockels cell switching using avalanche transistors", *Rev. Sci. Instruments* **77** (2006).
- [67] A. Marinoni, C. Moeller, J. Rost, M. Porkolab, and E. Edlund, "A pockels cell enabled heterodyne phase contrast imaging diagnostic for detection of ion cyclotron emission", *Rev. Sci. Instruments* **93** (2022).
- [68] N. Chen, X.-J. Wang, K. Liu, N. Zong, A.-N. Zhang, X.-M. Zhang, and Q.-J. Peng, "1.9 μ j external-

- cavity dumped ultra-broad-area semiconductor nanosecond laser”, *Opt. Lett.* **48**, 3555–3558 (2023).
- [69] C.-W. Lee and H. Jeong, “Quantification of macroscopic quantum superpositions within phase space”, *Phys. Rev. Lett.* **106**, 220401 (2011).
- [70] H. Jeong, M. Kang, and H. Kwon, “Characterizations and quantifications of macroscopic quantumness and its implementations using optical fields”, *Opt. Commun.* **337**, 12–21 (2015).
- [71] B. Hacker, “Two-photon gate and creation of optical cat states using one atom in a cavity”, Ph.D. thesis, TU München (2019).
- [72] C. Y. Hu, A. Young, J. L. O’Brien, W. J. Munro, and J. G. Rarity, “Giant optical Faraday rotation induced by a single-electron spin in a quantum dot: Applications to entangling remote spins via a single photon”, *Phys. Rev. B* **78**, 085307 (2008).
- [73] C. W. Gardiner, and M. J. Collett, “Input and output in damped quantum systems: Quantum stochastic differential equations and the master equation”, *Phys. Rev. A* **31**, 3761 (1985).
- [74] D. F. Walls, and G. J. Milburn, *Quantum Optics* (Springer-Verlag, Berlin, 1994).
- [75] S. Daiss, S. Langenfeld, S. Welte, E. Distant, P. Thomas, L. Hartung, O. Morin, G. Rempe, “A quantum-logic gate between distant quantum-network modules”, *Science* **371**, 614 (2021).
- [76] S. Welte, P. Thomas, L. Hartung, S. Daiss, S. Langenfeld, O. Morin, G. Rempe and E. Distant, “A nondestructive Bell-state measurement on two distant atomic qubits”, *Nature Photonics* **15**, 504 (2021).
- [77] Y. Liu, W.-J. Zhang, C. Jiang, J.-P. Chen, C. Zhang, W.-X. Pan, D. Ma, H. Dong, J.-M. Xiong, C.-J. Zhang, H. Li, R.-C. Wang, J. Wu, T.-Y. Chen, L. You, X.-B. Wang, Q. Zhang, and J.-W. Pan, “Experimental Twin-Field Quantum Key Distribution over 1000 km Fiber Distance”, *Phys. Rev. Lett.* **130**, 210801 (2023).